HHS Public Access

Author manuscript

Nat Biotechnol. Author manuscript; available in PMC 2024 August 02.

Published in final edited form as:

Nat Biotechnol. 2024 March ; 42(3): 437–447. doi:10.1038/s41587-023-01900-x.

Generation of precision preclinical cancer models using regulated *in vivo* base editing

Alyna Katti[1,2,*], **Adrián Vega-Pérez**[1,*], **Miguel Foronda**[1,7], **Jill Zimmerman**[1,2], **Maria Paz Zafra**[1,8], **Elizabeth Granowsky**[1], **Sukanya Goswami**[1], **Eric E. Gardner**[1], **Bianca J. Diaz**[1,2], **Janelle M Simon**[4], **Alexandra Wuest**[4], **Wei Luan**[4], **Maria Teresa Calvo Fernandez**[1], **Anastasia P. Kadina**[5], **John A Walker II**[5], **Kevin Holden**[5], **Scott W. Lowe**[4,6], **Francisco J. Sánchez Rivera**[4,9,10], **Lukas E. Dow**[1,2,3,#]

[1.]Sandra and Edward Meyer Cancer Center, Weill Cornell Medicine, New York, NY, USA

[2.]Graduate School of Medical Sciences, Weill Cornell Medicine, New York, NY, USA

[3.]Department of Medicine, Weill Cornell Medicine, New York, NY, USA

[4.]Cancer Biology and Genetics, Memorial Sloan Kettering Cancer Center, New York, NY, USA

[5.]Synthego Corporation, Redwood City, CA, USA

[6.]Howard Hughes Medical Institute, Memorial Sloan Kettering Cancer Center, New York, NY, USA

[7.]Current affiliation: Memorial Sloan Kettering Cancer Center, New York, NY, USA

[8.]Current affiliation: Biosanitary Research Institute (IBS) - Granada, Granada, Spain

[9.]Current affiliation: David H. Koch Institute for Integrative Cancer Research, Massachusetts Institute of Technology, Cambridge, 02142, Massachusetts, USA

[10.]Current affiliation: Department of Biology, Massachusetts Institute of Technology, Cambridge, 02142, Massachusetts, USA

Abstract

Although single nucleotide variants (SNVs) make up the majority of cancer-associated genetic changes and have been comprehensively catalogued, little is known about their impact on tumor initiation and progression. To enable the functional interrogation of cancer-associated SNVs, we develop a mouse system for temporal and regulatable *in vivo* base editing (iBE). The iBE mouse carries a single expression optimized cytosine base editor transgene under the control of a tetracycline response element (TRE) and enables robust, doxycycline-dependent expression across a broad range of tissues in vivo. Combined with plasmid-based or synthetic guide RNAs, iBE drives efficient engineering of individual or multiple SNVs in intestinal, lung, and pancreatic organoids. Temporal regulation of BE activity allows controlled sequential genome editing ex vivo

[#]Correspondence to: lud2005@med.cornell.edu.
[*]These authors contributed equally

Authors' contributions:

A.K. and A.V.P. designed and performed experiments, analyzed data and wrote the paper. M.F., J.Z., M.P.Z., S.G., E.G., J.S. and W.L, B.J.D., M.C.F., K.H., and F.J.S-R., performed experiments and/or analyzed data. S.W.L. supervised experimental work. L.E.D designed and supervised experiments, analyzed data and wrote the paper.

and in vivo, and delivery of sgRNAs directly to target tissues facilitates generation of *in situ* pre-clinical cancer models.

Missense and nonsense mutations represent the vast majority of disease-associated genetic changes[1, 2]. Cancer cells often harbor thousands of single base pair substitutions[3] and understanding the impact of specific variants is critical for defining disease drivers and highlighting therapeutic vulnerabilities. While many model systems rely on gene 'knockout' or overexpression studies to interrogate the role of specific genes in disease states, ample evidence suggests that individual single nucleotide variants (SNVs), even within the same gene[4–7] or codon[8], can dictate unique cancer phenotypes and response to targeted therapies.

Mice and organoids are powerful pre-clinical model systems, yet engineering cancer-associated SNVs in these complex settings is still laborious and inefficient. Cytosine and adenine base editing (CBE and ABE, respectively) offer the most efficient approach to create targeted (C:G to T:A or A:T to G:C) SNVs[9–12]; however, efficient *in vivo* BE requires robust expression of editing enzymes that is limited by adequate delivery and can induce antigen-driven immune responses[8, 13–20]. Improving the ease, efficiency, and control with which BE and SNVs can be generated in complex cell systems will streamline the functional annotation of disease-associated genetic changes.

Here, we describe a mouse model carrying an expression optimized, inducible, and regulated cytosine base editor (BE3RA[8]) to enable temporal control of BE in a wide variety of murine tissues. We show that inducible and transient expression of a single integrated BE enzyme (iBE) is capable of driving highly efficient base editing in pancreatic, lung, and intestinal organoids. Further, we demonstrate that iBE can be used in combination with somatic sgRNA delivery, to build *in vivo* pre-clinical models of hepatocellular carcinoma (HCC) and pancreas ductal adenocarcinoma (PDAC) harboring single or multiple specific cancer-associated SNVs. In all, iBE is a unique tool for efficient modeling of SNVs in physiologically accurate preclinical models to define and test their impact in tumor initiation and progression.

Results

Tightly regulated *in vivo* expression of an optimized base editor

To derive mice carrying an inducible base editing (iBE) allele, we injected KH2 mouse embryonic stem cells (ESCs) harboring a single copy of an expression optimized TRE-BE3RA transgene downstream of the *Col1a1* locus[8] (Figure 1a, Extended Data Fig. 1a,b) into albino B6 blastocysts. High-chimerism (agouti) founders were then backcrossed to C57Bl/6 mice for at least 4 generations before analysis. In the absence of doxycycline (dox), the iBE allele transmitted at normal Mendelian ratios and could be maintained as a heterozygous or homozygous colony (Supplementary Table 1, Extended Data Fig. 1c). We have previously shown that induction of doxycycline (dox)-regulated transgenes at the *Col1a1* locus with a constitutively expressed third-generation reverse tet-transactivator (CAGs-rtTA3) allele drives uniform expression across a broad range of murine cell types, particularly epithelial tissues[21, 22]. To evaluate expression in the iBE mouse, we generated

CAGs-rtTA3$^{+/-}$;iBE$^{+/-}$ (iBE hemizygous or "iBE^{hem}") mice and fed them dox chow (200 mg/kg) for one week. All tissues examined showed dox-dependent induction of BE3RA that could be reversed following dox withdrawal (dox switched, or 'SW') (Figure 1b). No tissues showed evidence of BE protein expression in the absence of dox, though RNA sequencing of intestinal tissue revealed a low, but detectable amount of BE3RA transcript (~1/1M transcripts) (Figure 1d). Unlike the uniform induction seen in GFP-shRNA transgenes at the *Col1a1* locus[21, 22], BE3RA appeared heterogeneous across multiple tissues (Figure 1c, Extended Data Fig. 1e). We reasoned this was likely due to stochastic silencing of either CAGs-rtTA3 or iBE during embryogenesis. To test this, we generated mice carrying one or two copies of each allele and examined expression across a range of tissues (Extended Data Fig. 2). The presence of two rtTA3 alleles (CAGs-rtTA3$^{+/+}$;iBE3$^{+/-}$) increased the uniformity of BE3RA expression, and this was further improved in mice carrying two iBE alleles (CAGs-rtTA3$^{+/-}$; iBE$^{+/+}$) (Extended Data Fig. 2). As expected, CAGs-rtTA3$^{+/+}$;iBE$^{+/+}$ ("iBE^{hom}") mice showed the most consistent and uniform expression of BE3RA across liver, pancreas, small intestine, and colon (Figure 1c,d, Extended Data Fig. 1e). Despite increased overall expression in iBE^{hom} animals, transcript and protein expression returned to baseline within one week of dox withdrawal (Figure 1c,d). RNAseq analysis revealed minimal change to cellular transcriptomes in the intestine and liver of iBE^{hom} mice, with no pattern of differential gene expression associated specifically with induction of the BE enzyme (Figure 1e,f, Supplementary Table 2), with the largest expression change being the BE enzyme itself (Figure 1e, Supplementary Table 2). Consistent with this data, no histological abnormalities or differences in immune cell populations were observed in iBE^{hom} animals treated with or without dox for two weeks (Extended Data Fig 3a,b).

Minimal off-target RNA and DNA editing in iBE mice

Previous studies have reported that BE enzymes can produce widespread, sgRNA-independent off-target RNA editing [23]. To determine if RNA editing could be a concern in iBE mice, we analyzed mRNA from the liver and intestine of iBE^{hom} mice (or CAGs-rtTA3 only controls) treated with or without dox for 2 weeks and those treated for 2 weeks and withdrawn from dox for 6 days. Analysis of transfected HEK293T cells from previously published data [23] showed a dramatic 280-fold increase in C>U edited RNA transcripts (1880 C>U variants/1M reads) relative to control (~7 C>U variants/1M reads)(Extended Data Fig. 4a). Similarly, muscle tissue from recently published transposon-based BE3 transgenic mice [24] showed a 30-fold increase in C>U variants (~380 vs ~12 C>U variants/1M reads) (Extended Data Fig. 4a). In comparison, iBE^{hom} tissues showed much lower levels of C>U RNA editing in liver (~36 C>U variants/1M reads) and intestine (~19 variants/1M reads) in dox treated samples, representing a 6-fold and 3-fold increase over controls, respectively. Further, this moderate increase was almost entirely reversed within 6 days of withdrawing dox chow (Extended Data Fig. 4a). Non-C>U editing levels remained unchanged over all conditions (Extended Data Fig. 4b). One possible explanation for the difference in editing frequency between our model and previous reports, is the relative level of BE enzyme expression between experimental systems. Indeed, BE3 transcript was ~70-fold higher in transfected HEK293T cells than dox-treated iBE tissues (Extended Data Fig. 4c).

In addition to RNA editing, we assessed the possibility of DNA off-target effects using iBE targeted ESCs expressing *Apc*^{Q1405} and *Pik3ca*^{E545K} sgRNAs. Using ESCs enables the reliable growth and isolation of clonal populations following iBE induction by dox treatment to ensure any infrequent mutations can be detected. In total, we assessed 60 dox-treated clones and 60 no dox control clones (in pools of 10) using ultra deep sequencing (800–1000x coverage) of a focused panel of cancer-relevant genes (MSK-IMPACT [25]). We saw no evidence of increased C>T DNA editing in dox treated cells relative to controls (Extended Data Fig. 5, Supplementary Table 3).

Together, these data show that the iBE transgene can be induced and repressed uniformly across a range of murine tissues and that low levels of C>U RNA editing can be quickly reversed by withdrawal of transgene expression.

Efficient single and multiplexed editing in iBE organoids

Organotypic cell culture models or ‘organoids’ are a powerful systems to study epithelial biology. We and others have used organoids to reveal the contribution of cancer-associated nonsense and missense mutations for cell behavior and drug response [26, 27]; however, efficient introduction of SNVs using base editing is a substantial practical challenge in scaling up the generation of large collections of tailored model systems. To determine if cells derived from iBE mice could streamline the creation of targeted mutations *ex vivo*, we generated organoids from small intestine, pancreas, and basal cells from the trachea of iBE mice. Each culture showed robust inducible and reversible expression of BE3RA (Supplementary Figure 1a), and organoids transduced with the BE-activatable GFP^{GO} reporter [28] showed editing efficiencies ranging from 40–90% (Figure 2a,b, Supplementary Figure 6b), with minimal impact on the organoid transcriptome, and no detectable off-target RNA editing observed up to 8 days on dox (Extended Data Fig. 6).

To closely assess editing dynamics, we generated multiple independent iBE^{hom} pancreatic organoid cultures carrying the *LSL-Kras*^{G12D} allele and generated *Kras*^{G12D};*p53*^{Q97X} (KP) mutant organoids by nucleofecting dox-treated cells with synthetic sgRNA and tat-Cre protein; KP cultures survive serial passaging more efficiently and expand faster than WT organoids, simplifying serial measurements over multiple time points. GFP^{GO}-transduced KP organoids showed 1–2% editing in the absence of dox, but induced target editing and GFP expression rapidly following dox treatment. Two days following dox exposure more than 50% of cells were GFP positive, with maximal editing (70–80% GFP positive) occurring at approximately 3–4 days (Figures 2c,d Extended Data Fig.7a). Transient exposure to dox for only 2hrs or 12hrs resulted in sub-maximal editing (55% and 70% of max respectively), supporting the notion that BE enzyme expression and editing are both quickly induced and rapidly suppressed following dox withdrawal (Figures 1d and 2d). Re-exposure to dox in these cells recovered maximal editing efficiency at similar kinetics to that seen in dox-naïve cultures (Figure 2d and Extended Data Fig.7a). Consistent with the GO reporter, endogenous target editing with an Apc.Q1405 targeting sgRNA showed similar kinetics, being detectable 12h after dox addition and reaching 80% of total BE within 48hrs. (Extended Data Fig.7b). Consistent with previous experience with this sgRNA, indels were

rare at D3 (~1% total reads) but increased 4-fold when maintained on dox over 3 weeks (Extended Data Fig.7c).

We next asked whether iBE could improve the efficiency of building complex organoid-based models of cancer. To limit the introduction of exogenous and potentially immunogenic components we opted for transient transfection of sgRNAs by nucleofection. Organoids were cultured in dox-containing media for 2 days before and after nucleofection (4 days total) to transiently induce the editor and align BE protein expression with sgRNA expression; Editing was quantified 7d post-transfection by target amplicon sequencing. Nucleofection of the *Apc*^{Q1405X} sgRNA in a U6 expression plasmid (LRT2B[8]) induced ~50% target editing, while *Trp53*^{Q97X} and *CR8*^{OS2} gRNAs consistently showed C>T editing below 5% (Figure 2e). In contrast to plasmid-based delivery, nucleofection of dox-treated organoids with chemically stabilized synthetic sgRNAs led to significantly higher editing, up to 43-fold higher in the case of CR8^{OS2} (Figure 2e, Extended Data Fig. 8a). Notably, editing with the iBE transgene was 40–100+ fold higher than nucleofection of WT organoids with synthetic sgRNAs and an optimized BE (FNLS) cDNA plasmid (Figure 2e), highlighting the improved workflow using iBE organoids.

Using the more efficient synthetic sgRNA approach, we next tested a range of additional BE sgRNAs predicted by BE-SCAN (https://dowlab.shinyapps.io/BEscan/)[29] to effectively induce targeted SNVs. In unselected populations, 7d post-transfection, C>T editing efficiencies ranged from ~20%−90% (Figure 2f). Functional selection for mutant organoids (RSPO withdrawal for Ctnnb1^{S33F}, or TGFβ for Smad4^{Q224X}, Nutlin3 treatment for p53 mutations, and Selumetinib treatment for Pik3ca^{E545K}) enriched C>T editing 80–95% for tumor suppressor (*Smad4* and *Trp53*) and 50–80% for oncogenes (*Pik3ca* and *Ctnnb1*) (Figure 2f, Extended Data Fig. 8b). Most guides showed minimal (bystander) editing of adjacent cytosines that would result in additional amino acid substitutions (Figure 2g, Extended Data Fig. 8c-j and Extended Data Fig. 9). The only notable exceptions to this were sgRNAs targeting *Trp53.V197M*, in which 20% of alleles carried an adjacent R196Q mutation (Extended Data Fig. 8e), and the *Trp53.Q97X* sgRNA that uniformly harbored an S96F alteration immediately before the premature termination codon (Extended Data Fig. 8c). In the latter case, the predicted functional impact on the truncated p53 protein is minimal.

Given the high efficiency of engineering individual target mutations, we next asked whether iBE organoids could be used for rapid multiplexed editing. Using iBE^{hom} organoids to maximize the likelihood of efficient enzyme expression in all cells, we delivered a combination of four sgRNAs - *Apc*^{Q1405}, *Trp53*^{C135Y}, *Smad4*^{Q224X}, and *Pik3ca*^{E545K} - to model frequently observed colon cancer mutations; notably, three of the four sgRNAs used show moderate single editing efficiency (20–45%), thereby providing a test of multiplexed editing in non-ideal circumstances. Target editing for each site in the bulk, unselected populations resembled that seen with individual transfections in iBE^{hem} cells (Figure 2h, Supplementary Figure 2a) and iterative functional selection for each mutation resulted in an organoid population with ~80–90% C>T editing for *Apc*, *Trp53*, and *Smad4* (Figure 2i, Supplementary Figure 2b), while *Pik3ca*^{E545K} editing reached ~65%, consistent with the notion that heterozygous mutations are sufficient to activate PI3K signaling. Control

organoids receiving all 4 sgRNAs in the absence of dox showed <1% editing and did not survive functional selection (Figure 2h, Supplementary Figure 2a). Together, these data show that iBE provides an efficient system for engineering disease relevant SNVs and can be used to quickly generate genetically complex cancer models.

iBE enables sequential base editing *in vitro* and *in vivo*.

One powerful application of inducible BE technology is the potential for temporally separated or sequential editing. To test the feasibility of this approach, we cultured *ex vivo* edited, transformed Apc^{Q1405X}, $p53^{C135Y}$, $Smad4^{Q224X}$, $Pik3ca^{E545K}$ (APSP) mutant intestinal organoids (Figure 3a) in the absence of dox to suppress expression of the base editor and transduced the cells with the lentiviral GFP^{GO} reporter. Selected organoids maintained in the absence of dox showed minimal editing (<1%), whereas 4 days of dox treatment led to ~50% target editing (Figure 3b,c)., consistent with primary, untransformed organoids (Figure 2a,b). To determine whether this system could be used to control the timing of gene editing *in vivo*, we engrafted APSP intestinal organoids into recipient animals, either sub-cutaneously or into the liver (via intrasplenic injection) to mimic metastatic disease (Figure 3a). Once tumors had formed (10 days following subcutaneous transplant or 8 weeks following intrasplenic delivery), mice were treated with dox (200mg/kg in chow) for 7 days and tumors collected for analysis. As expected, subcutaneous tumors expressed nuclear-localized mScarlet, while only the dox-treated mice showed robust GFP fluorescence throughout the tumor mass (Figure 3d,e). Similarly, dox-treated liver 'metastases' showed widespread GFP activation compared with non dox-treated control animals (Figure 3g). Flow cytometry analysis showed editing efficiencies up to 40%, with low levels of leaky GFP activation, even after 8 weeks of in vivo tumor growth (Figure 3f,h).

iBE enables precise somatic editing in the liver.

We and others have previously used transfection and viral-based delivery of base editors to generate somatic mutations in mouse hepatocytes, *in situ* [8, 13–20]. Though remarkably effective in liver, somatic delivery of Cas9-based enzymes can result in antigen-mediated immune responses[30–32]. As a first step to measure whether *in vivo* somatic editing with the iBE allele could be used to derive tumor models, we used hydrodynamic tail vein injection (HTVI) to introduce a *Myc* cDNA in a sleeping beauty (SB) cassette (*SB-Myc*) as well as sgRNAs targeting *Apc*, *Ctnnb1*, or *Trp53* designed to engineer known cancer-linked SNVs [8, 33, 34]. To drive BE enzyme expression, iBE mice were maintained on dox for one week prior to injection and one-week post- injection (Figure 4a); Six weeks following HTVI, tissue was harvested for sequencing and histological analysis (Figure 4a). Most mice (12/13) injected with SB-*Myc* and a control sgRNA targeting a non-genic region (CR8) had no macroscopically visible tumors, but showed small, well-circumscribed regions on histological sections, which were also observed in *SB-Myc* only animals (Figure 4b). Consistent with an established role for WNT signaling in a subset of HCC [8, 33, 34], *SB-Myc;*Apc^{Q1405X} and *SB-Myc;*$Ctnnb1^{S33F}$ mice showed markedly enhanced tumor growth (5/6 and 4/6 mice, respectively) (Figure 4b). Targeted amplicon sequencing revealed a high proportion of expected SNVs, with low rates of insertions or deletions (indels) (Supplementary Figure 3a-e). Absolute editing rates in bulk tumor tissue were

variable, likely due to the presence of admixed stroma and immune cells (Figure 4c and Supplementary Figure 3a-c). Notably, *SB-Myc;Ctnnb1*^{S33F} tumors showed lower overall editing rates that *Apc*^{Q1405X} mutant tumors, consistent with the notion that heterozygous *Ctnnb1*^{S33F} mutations are sufficient to activate WNT signaling, while *Apc* requires inactivation of both alleles. Both *Apc*^{Q1405X} and *Ctnnb1*^{S33F} tumors showed accumulation and mislocalization of β-catenin protein and elevated expression of glutamine synthetase (GS), a WNT target that is normally restricted to pericentral hepatocytes surrounding the central vein (Figure 4b). Consistent with a strong tumor suppressive role for p53 in HCC, introduction of an sgRNA targeting *Trp53* (Trp53.C135Y) accelerated tumor growth, with 5/7 mice showing multi-focal tumors, and high levels of on-target editing (Figure 4b,c and Supplementary Figure 3d). Like previously characterized p53 hotspot mutations[35–38], C135Y resulted in p53 protein stabilization and nuclear localization (Figure 4b,c and Supplementary Figure 3d). Interestingly, despite detectable editing within macroscopic tumor nodules (Figure 4b), most M237I sgRNA transfected livers showed small lesions resembling those seen with Myc alone, with isolated regions of each tumor showing elevated nuclear staining for p53 (Figure 4b).

Given the reduced tumor penetrance in Myc/p53^{M237I} transfected livers, we asked whether addition of a second oncogenic mutation could be combined to enable tumor growth with this p53 alteration. Delivery of two sgRNAs (*Trp53*^{M237I} and *Ctnnb1*^{S33F}) drove tumor growth in all mice analyzed (4/4) with detectable editing in both target loci. These tumors showed increase CTNNB1 protein and WNT target (GS) expression. Like M237I alone, dual-edited tumors showed sporadic nuclear p53 staining (Figure 4e,d, Supplementary Figure 4). To confirm that the editing of both loci was occurring within the same cells of the tumor, we derived 4 cell lines from individual tumor nodules from two different animals. This analysis revealed editing and mutational activation of β-catenin in each of the four cell lines, with tumor line #4 showing a non-canonical C>A conversion, consistent with the frequency of editing outcomes seen previously with this sgRNA (Fig 4f) [28]. Two of four lines contained homozygous p53^{M237I} editing, while in the remaining two showed heterozygous p53^{M237I} alterations, in line with reduced editing observed in single sgRNA experiments, and perhaps explaining the variability of nuclear p53 staining (Supplementary Figure 4).

In an effort to improve the efficiency of developing *in vivo* models with iBE and eliminate the need for sgRNA cloning, we tested the delivery of chemically stabilized, non-encapsulated (‘naked’) synthetic sgRNAs. Like plasmid delivery, synthetic sgRNAs targeting *Apc, Ctnnb1* or *Trp53* coupled with *SB-Myc* drove consistent tumor formation in the liver following HTVI (Extended Data Fig. 10a,b). For both nonsense (*Apc*^{Q1405X} and *Trp53*^{Q97X}) and missense (*Ctnnb1*^{S33F}) mutations, we saw high on-target C>T editing and low indel formation (Supplementary Figure 3g-i).

Together, these data show that the iBE mouse enables temporally regulated target editing and can be used to generate *in vivo* liver cancer models through controlled and precise induction of cancer-relevant SNVs.

Engineering oncogenic missense mutations in the pancreas

To test the potential for using iBE in the generation of *in situ* cancer models in tissue other than liver, we used an electroporation-based approach[39, 40] to introduce a targeted mutations into the mouse pancreas combined with an SB cassette that expresses $Kras^{G12D}$ (*SB-Kras*) (Figure 5a). iBE^{hem} mice targeted with *Trp53* gRNAs showed rare incidence of tumor development (1/10 mice; however, iBE^{hom} mice showed induction of large pancreatic tumors in 4/7 mice by 5–8 weeks (Figure 5b, Supplementary Figure 5a,b). Like genetically engineered Kras;p53 driven Cre models (KPC)[35], tumors contained $CK19^{+}$ ductal islands with substantial surrounding stroma expressing alpha-smooth muscle actin (α-SMA, Figure 5b). Sequencing of bulk tumors revealed precise on-target C>T editing with minimal indels. Absolute editing percentages from bulk tumor were low, likely due to the abundance of non-tumor cells, as frequently observed in human and mouse PDAC (Figure 5c). Electroporation of the pancreas with SB-$Kras^{G12D}$ and synthetic *Trp53.Q97X* sgRNAs in iBE^{hom} mice showed highly penetrant tumor growth (5/6 mice), efficient C>T editing and identical histology to what was observed with plasmid-based delivery (Figure 5c, Supplementary Figure 5b-c). Finally, following the same paradigm used previously in the liver, we generated genetically complex PDACs *in vivo* by multiplexed delivery of *SB-Kras* and sgRNAs targeting both *Trp53.Q97* and *Pik3ca.E545* (Figure 5d). All tumors showed evidence of editing at both target sites, at levels consistent with that observed for individual sgRNAs (Figure 5e, Supplementary Figure 5d). Moreover, dual $Trp53^{Q97X}$ and $Pik3ca^{E545K}$ edited tumors showed elevated levels of pAKT compared with $Trp53^{Q97X}$ only tumors, consistent with mutation-driven activation of the PI3K/AKT pathway (Figure 5f). Thus, iBE mice provide a platform for rapid and easy generation of disease-associated SNVs in multiple organ sites *in situ*.

Discussion

The generation of model systems that faithfully recapitulate the genetic alterations observed in human disease is a key step in developing precision treatment strategies. Here, we set out to produce an efficient and regulated platform to streamline the creation of such pre-clinical disease models. The iBE platform enables efficient creation of targeted nonsense and missense mutations *in vivo* in somatic tissues, and in cells and organoids derived from mice. Further, the system supports multiplexed and/or sequential editing with synthetic sgRNAs, thus providing a rapid approach to engineer complex genetic combinations often seen in human cancers.

Previous work has demonstrated the potential of *in vivo* BE for engineering SNVs[8, 13–20], though these approaches have relied on exogenous delivery of BE enzymes using transfection, split inteins in AAV vectors, or engineered virus like particles (eVLPs). These approaches can catalyze highly efficient editing in a subset of tissues (i.e. the liver, muscle, brain, and eye)[8, 13–20], though may suffer from unintended immune recognition of Cas9-derived antigens[30–32]. iBE broadens the number of tissues that can be targeted with CBEs for disease modeling and as it is encoded in the genome, may avoid complications of immunogenicity when induced in somatic tissues. We cannot rule out a potential immune response to exogenously delivered sgRNA expression vectors, or even naked sgRNA, though

to our knowledge such responses have not been reported. Annunziato et al previously described a genomically-encoded Cre-activatable BE mouse using the pre-optimized BE3 enzyme[41]. This transgenic mouse demonstrated the ability to induce target editing in the mammary gland and drive tumor development in combination with Myc; however, perhaps due to the sustained expression of BE3 from a constitutive promoter, target sites often accumulated indels rather than desired SNVs[41]. In the present study, we saw minimal indel formation across 10 different target sites both *in vitro* and *in vivo*. Yet, as expected, we saw a modest accumulation of indels in cells maintained on dox over 3 weeks in culture. Thus, the reversible induction of enzyme expression in iBE provides a key improvement that limits indel formation at endogenous genomic targets.

Our goal was to develop a system for creating precise, genetically-defined pre-clinical models. One recent study described the generation of constitutive BE3 transgenic mice using *piggybac* transposition and reported high levels of off-target DNA and RNA editing throughout the genome and transcriptomes of these mice, respectively [24]. We thoroughly explored sequence-independent DNA and RNA off-target effects following dox induction in iBE cells and tissues. Rather than performing whole genome sequencing on a small number of post-editing clones, we opted for targeted deep sequencing of cancer-relevant genes contained in the MSK-IMPACT panel[25]. While this approach does not measure editing across the entire genome, it enabled the analysis of 120 individual ESC clones. We saw no increase in APOBEC-mediated (C>T) mutation profile in dox treated samples, suggesting that iBE does not induce widespread sequence-independent DNA off-targets in cancer-associated genes, but we cannot rule out the possibility of rare mutations elsewhere in the genome. It is likely that limiting dox exposure through transient induction of the editing enzyme avoids many of the unwanted genomic edits described in other studies.

Similarly, and in contrast to published data [23, 42], we saw no evidence of sequence-independent off-target RNA editing in pancreatic organoids on dox for 8 days, and only 3–6 fold increase in RNA variants in intestinal and liver tissue from mice treated with dox for 2 weeks. In fact, RNA editing in iBE mice was 10-fold lower than reported by Yan et al [24], and 100-fold lower than observed in HEK293 transfected cells [23] (Extended Data Fig.4). As described for off-target DNA editing, we believe it is likely that the relatively modest level of enzyme expression from the single copy transgene can maintain on-target DNA editing while minimizing potential off-target effects (Supplementary Figure 4). Moreover, withdrawal of dox for 6 days in iBE animals reversed already low RNA editing to baseline levels, implying that the observed editing was not reflective of permanent DNA mutagenesis, but is transient and can be minimized through shortening the window of BE enzyme induction. Together, these observations suggest most reported off-target consequences of BE enzymes can be mitigated by carefully regulating the duration and absolute level of BE enzyme expression, highlighting the utility of iBE mice for preclinical disease modeling.

Accurate genetic disease modeling in the mouse involves both targeting the correct cell populations and engineering precise genomic changes in those cells. In this study, we used iBE animals in which expression of the BE enzyme was induced throughout the body and restricted delivery of the sgRNAs to specific tissues. In situations where sgRNA delivery cannot be directed to a specific tissue or cell population of interest, induction

of the BE enzyme can be restricted to specific compartments by combining iBE with well-characterized cell or tissue restricted rtTA or Cre drivers. This would enable broad delivery of sgRNAs (e.g via AAV) by restrict editing to those cells expressing the BE transgene. To produce precise SNVs or single amino acid substitutions, sgRNA selection is critical. We used a range of sgRNAs from a pre-validated collection [29] that estimates editing purity. As shown in Figure 2, in most cases, it is possible to achieve highly precise target editing in bulk populations, but the use of prediction tools [43–46] or empirically tested collections [29, 47] will help maximize efficiency and minimize unwanted bystander editing. There will be situations in which the presence of adjacent cytosines restricts the ability of iBE to produce single precise amino acid changes. Further, while C>T mutations represent the most frequent cancer-associated variants, specific disease models may require different base substitutions. In these cases, the use of genome editing approaches such as *in vivo* HDR [48] or prime editing [49, 50] provide a strategy to overcome the limitations of BE, though increased flexibility may come at a cost of targeting efficiency.

Our proof-of-concept studies demonstrate the utility of the iBE platform for *ex vivo* and *in vivo* target editing. Further, given the broad expression of iBE across all tested tissues, and the ability to control timing and tissue distribution of BE activity, the model is a powerful tool to engineer and study missense mutation *in vivo* for many disease applications.

Methods

Animals

All animal experiments were approved by the Weill Cornell Medicine Institutional Animal Care and Use Committee (IACUC) under protocol 2014–0038 or by the MSKCC Institutional Animal Care and Use Committee under protocol 11–06–018. ES cell-derived mice were produced by injection into albino B6 blastocyst by the transgenic targeting core facility at NYU School of Medicine. High chimera (agouti) founders were backcrossed to C57Bl/6 mice for at least 4 generations before analysis. iBE^{het} mice were generated through breeding with C57Bl/6 mice containing a R26-CAGs-rtTA3 allele (Supplementary Table 1). iBE^{hom} mice were generated through breeding iBE^{het} progeny. Animals will be made available at Jackson Laboratories under strain designation B6.Cg-*Col1a1*$^{tm1(tetO\text{-}cas9*)Ldow}$/Mmjax (JR#037818). Mice were genotyped by Col1a1[51], R26, and CAGs-rtTA3 PCRs using EconoTaq PLUS (Lucigen #30033–2). Doxycycline chow (food pellets) were administered for 1 or 2 weeks (as specified) at 200mg/kg (Envigo #TD.180625). Mice were manipulated experimentally (organoids, injection, or electroporation) at 8–12 weeks of age. Male and female mice were used for all studies.

Cloning

All plasmid sgRNAs were cloned into the BsmBI site of LRT2B[8]. Oligos for gRNA cloning are found in Supplementary Table 4.

ES cell targeting

KH2 mouse embryonic stem cells (ESCs) harboring a TRE-BE3RA transgene at the Col1a1 locus were engineered as previously described[8]. Briefly, the BE3RA cDNA from Lenti-

BE3RA was cloned into the *Col1a1* targeting vector containing a TRE-promoter element (cT)[51].

Taqman copy number assay

After gDNA isolation using the Qiagen blood and tissue kit, copy number assays were performed using the TaqMan Copy Number Assay (Thermo Fisher #4400291) following the manufacturer's instructions.

Cells

HEK293T (ATCC CRL-3216) cells were purchased from the ATCC. Stocks were tested for mycoplasma routinely every 6 months and maintained in Dulbecco's Modified Eagle's Medium (DMEM, Corning # 10–013–CV) containing 1% Pen/Strep (Corning #30–002–Cl) and 10% FBS at 37C with 5% CO_2.

Organoid culture and transduction

Murine small intestine organoids from the indicated genotypes were isolated and maintained as previously described[52]. Isolation of murine pancreatic ductal organoids was done modifying previously described protocol[53, 54]. Isolation of murine pulmonary basal cell spheroids was performed using tracheas pooled from 3 animals. Animals were euthanized by inhaled carbon dioxide, sprayed down with 70% ethanol and then sheathed. Following gross dissection of the thoracic cavity, animals were cardiac perfused with PBS through the left ventricle and tracheas were cut away from the bronchial tree, capping at the submucosal glands. Single cell suspensions were generated using a gentleMACS Octo Dissociator and a mouse lung dissociation kit (Miltenyi #130–095–927) on the m_lung_02 protocol. Crude suspensions were then passed through 70um mesh filters and rinsed with 10cc of cold FACS buffer (PBS + 2% FBS + 2mM EDTA). Cells were pelleted at 500g for 3min, red blood cells lysed for 3min using 5cc of ACK lysis buffer (Thermo Fisher #A1049201) and then quenched with 20cc of FACS buffer. Cell pellets were resuspended in FACS buffer, filtered through 70um cell strainer FACS tubes and counted (Nexcelom Cellometer Auto X4). Cd31/Cd45 cells were depleted using 10uL each of Cd31 (Miltenyi #130–097–418) and Cd45 (Miltenyi #130–052–301) microbeads per 10^7 total cells and passed through an LD depletion column (Miltenyi #130–042–901). Cells were seeded in a 6.5mm transwell insert at ~20K cells in 200uL of a 50% Matrigel suspension (BD Biosciences, 354230) per transwell. Matrigel/cell mix was incubated for 15 min at 37C to allow for solidification and base media with Primocin® (InvivoGen) was added to top and bottom chambers of transwell. Base media constitutes: DMEM/F12 + HEPES (15mM) + Sodium Bicarbonate (3.6mM) + L-glutamine (4mM)+ Insulin (10ug/mL) +Tranferrin (5ug/mL) (or ITS,1x, Sigma Aldrich #I3146) + Cholera Toxin (0.1ug/mL, Sigma Aldrich C9903) + EGF (25ng/mL)+ Bovine Pituitary Extract (30ug/mL, Sigma Aldrich, P1476)+ FBS (5%) + Retinoic Acid (0.05uM). During the first 48hrs of seeding or passage, 1uM Y-27632 (MedChemExpress; HY-10583) was added to the base media. Media was changed every 2 days and cells were passaged after ~1 week and every ~3–4 days for subsequent passages. Organoids were transduced as previously described.

Tumor implantation

Tumor organoids isolated from CAGs-rtTA3^{hom} / iBE^{hom} mice (engineer to contain 4 oncogenic single nucleotide variants) were engrafted into the flanks (sub-cutaneous injection) or livers (intrasplenic injection) of recipient mice. Sub-cutaneous tumors were allowed to grow for 10 days after injection and mice were treated with dox (200mg/kg in chow) for 1 week to induce BE expression. Flank tumors were imaged by IVIS (Perkin Elmer) using the appropriate filters to visualize GFP and mScarlet. Liver tumors were allowed to grow for 6–8 weeks after implantation and mice were treated with dox (200mg/kg in chow) for 1 week prior to analysis.

Tumor digestion

After isolation, tumors were digested with Collagenase IV (2000u/ml) and DNAse (10,000u/ml) in HBSS for 20 mins at 37C in a shaking water bath. Then cell suspensions were filtered through 40-μm cell strainers, washed, and resuspended in EDTA-containing PBS supplemented with 3% FBS after erythrocyte lysis by osmotic shock.

Spleen and bone marrow cell suspensions.

For the preparation of a single-cell suspension from bone marrow, femora and tibiae were remove and place into cold PBS. Collection of bone marrow cells was performed by flushing the shaft with 5ml using a 10ml syringe with a 16-gauge needle. For the preparation of single-cell suspension from the spleen, the spleen was crushed and filtered through 40-μm cell strainers. Both cell suspensions were washed and resuspended in EDTA-containing PBS supplemented with 3% FBS after erythrocyte lysis by osmotic shock.

Generation of 2D lines from organoids

To engineer immortalized 2D lines, 3D small intestinal organoids were transduced with a lentiviral all-in-one *Kras*^{G12D} cDNA and MultimiR tandem knockdown cassette (sh*Apc*-sh*Trp53*)[55]. After selection in media without RSPOI and Nutlin3 (10umol/L), organoids were split onto plates coated with Rat Collagen I in PBS (Gibco, #A10483–01, 30ng/mL) for 30 minutes at 37C prior to plating. Cells were passaged on Collagen coated plates 3–5 times and then split to plates without Collagen. 2D cells were transduced with lentivirus as previously described[28].

Flow cytometry

Cells were trypsinized and organoids were mechanically dissociated followed by TrypLE treatment at the indicated time point. Analysis of immune cell populations of spleen and bone marrow was performed after blocking Fc receptors by incubating with an anti-CD16/32 antibody (Biolegend, #101320) at 4°C for 15 min. The cells were subsequently stained with fluorophore-conjugated antibodies using CD4-PE (BD, #100408), CD8 PE-Cy7 (BD, #100710), CD19 PE-Cy7 (BD,115509), CD11b PE (BD, #101207), GR1 PE (BD, #108407), CD45-APC (BD, #103112) for 20 min at 4°C in FACS buffer (PBS/2%FBS/3mM EDTA) followed by staining with DAPI. Flow cytometry assays were carried out on a Thermo Fisher 2018 Attune NxT flow cytometer. At least 25,000 events from the single cell

population gating were recorded, and gates set as shown (Supplementary Figure 6). All experiments were performed in replicates from independent mouse lines as annotated.

Organoid Nucleofection

Three days before nucleofection organoids were split for one well in a 12 well plate per condition and cultured in full media (ENR; 50ng/mL EGF, Invitrogen, and 50nMol LDN-0193189, Selleck Chemicals + RSPOI conditioned media). Two days prior to nucleofection, media was changed to EN (50ng/mL EGF, Invitrogen, and 50nMol LDN-0193189, Selleck Chemicals) + Y-27632 (10umol/L) + CHIR99021 (5umol/L) and with or without doxycycline as noted (500ng/mL). On day of nucleofection, media is removed, and organoids mechanically dissociated in cold PBS by pipetting (50X). Organoid suspension was pelleted by spinning at 1200rpm for 4 min at 4C and resuspended in 100uL TrypLE (Invitrogen #12604) followed by incubation in bead bath at 37C for 5 mins. ~300uL of cold PBS was added followed by mechanical dissociation of organoids by pipetting (50X), and then washed with cold PBS. Per condition, nucleofection mix was prepared as follows: 16.4 uL Primary P3 Buffer (Lonza kit, #V4XP-3032), 3.6 Supplement 1 (Lonza kit, #V4XP-3032), and 1ug of plasmid DNA or 200pmol of chemically stabilized synthetic RNA (Synthego Corp.). For multiplexing experiments, total gRNA concentrations were kept constant and divided evenly by number of gRNAs in that condition. Pelleted organoids were resuspended in 20uL of nucleofection mix and transferred to electroporation chamber (Lonza kit, #V4XP-3032, 96-well format) for electroporation using Lonza X Unit Nucleofector under the [ES, mouse] protocol. Organoids were recovered in 70uL of media and washed once. Pelleted organoids were plated in original volume of Matrigel (BD Biosciences, 354230) and cultured in EN + Y-27632 + CHIR +/− dox media for 2 days and subsequently replaced with full media or selection conditions. Nucleofection of WT organoids followed the same protocol electroporating the synthetic sgRNAs and an optimized BE (FNLS) cDNA (Addgene #112671).

Organoid functional selection

To select for WNT activating mutations, exogenous RSPOI was removed from the media. To select for loss-of-function *Trp53* mutations, Nutlin3 (5umol/L) was added to the media and organoids were cultured for 10 days. To select for *Smad4* alterations, recombinant TGFB1 (5ng/mL) was added to the media and organoids cultured for 7 days. To select for *Pik3ca* activating mutations, Selumetinib (1ug/mL) was added to the media and organoids cultured for 14 days. Organoids were split as usual throughout selection conditions.

Genomic DNA isolation

Cells and organoids were dissociated and pelleted at the indicated time point. Cells were lysed as previously described [8]. Tumor nodules were micro-dissected and homogenized using a 5mm stainless steel bead (Qiagen, #69989) and a Tissue LyserII (Qiagen) in 150uL genomic DNA lysis buffer for 3 mins at a frequency of 30 hz/s and immediately cooled for 5 mins on ice. Tumor suspension was then lysed and gDNA isolated identical to cells[8].

PCR amplification for sequencing

Target genomic regions of interest were amplified by PCR using primers in Supplementary Table 2. PCR was performed with Herculase II Fusion DNA polymerase (Agilent Technologies, #600675) according to the manufacturer's instructions using 200 ng of genomic DNA as a template and under the following PCR conditions: 95C × 5 min, 95C – 0:30 → 57C – 0:30 → 72C – 0:20 × 39 cycles, 72C × 5 min. PCR products were confirmed using Qiaxel and purified using QIAquick PCR Purification Kit (Qiagen # 28106). PCR products were quantified by NanoDrop (Thermofisher Scientific Inc) and normalized to 20ng/uL in EB buffer. Targeted amplicon library preparation and NGS sequencing (MiSeq; 2 × 250bp) were performed at Azenta (previously GENEWIZ, Inc.) and analyzed using CRISPResso2. Raw MiSeq fastq files have been deposited in the sequence read archive (SRA) under accession SUB11797785.

Protein analysis

Organoids—A 6-well of organoids was collected in Cell Recovery Solution (Corning, #354253) and incubated on ice for 30min – 2 hours, washed with PBS 3 times to removed residual Matrigel. Organoid pellets were resuspended in 100uL RIPA buffer, and centrifuged at 500 x g at 4C to collect protein supernatant.

Tissue—A 2mg piece of each tissue was collected at indicated time points and immediately processed or snap frozen and stored at −80C. Tissue was homogenized in 150uL of RIPA buffer with protease and phosphatase inhibitors by bead homogenizer (Tissue LyserII, Qiagen) for 3 mins at a frequency of 30 hz/s and immediately cooled for 5 mins on ice. The following antibodies were used for western blotting analysis of organoids and tissues: Cas9 (Biolegend, #844301) (1:500, 4C overnight) and actin (Abcam ab49900) (1:10,000, 30 min RT).

RNA isolation and RNA sequencing

A 6-well of organoids was collected in 800uL Trizol (Invitrogen, 15596–026). The livers were removed and immediately homogenized for 15–20s in 4ml of Trizol using a handheld homogenizer (Omni International, TM12500643). The intestinal villi were isolated by scrapping using glass slides and resuspended in 3ml of Trizol. Samples were immediately processed or stored at −80. RNA was extracted according to the manufacturer's instructions. DNA contamination was removed through treatment with recombinant DNaseI (Roche Diagnostics, #04716728001) for 15 minutes at RT and column purification using Qiagen RNeasy Mini kit (#74106). cDNA was prepared from 1ug of RNA (quantified by NanoDrop, Thermofisher Scientific Inc). Weill Cornell Medicine's Genomics Core Laboratory checked RNA quality using a 2100 Bioanlyzer (Agilent Technologies), prepared the RNA library (TruSeq Stranded mRNA Sample Library Preparation kit (Illumina), and performed RNA sequencing (single end 75 cycles on a Illumina NextSeq 500). Raw fastq files have been deposited in the sequence read archive (SRA) under accession PRJNA859154.

RNAseq analysis

Raw FASTQ files were mapped to mouse (GRCm39) or human (GRCh38) reference genomes using STAR (v2.4.1d; default parameters) [56]. STAR count data was used for estimating differential gene expression using DESeq2 [57]. For data visualization and gene ranking, log fold changes were adjusted using *lfcShrink* in DESeq2. R (v3.6.1) and R Studio (v1.2.1335) was used to create all visualizations and principal component analysis. Volcano plots, heatmaps, and other visualizations were produced using the software packages:

Enhanced Volcano (https://bioconductor.org/packages/devel/bioc/html/EnhancedVolcano.html)

pheatmap (https://www.rdocumentation.org/packages/pheatmap/versions/1.0.12/topics/pheatmap)

ggplot2 (https://cran.r-project.org/web/packages/ggplot2/index.html)

Variant calling was performed using picard (https://broadinstitute.github.io/picard/) and GATK (https://gatk.broadinstitute.org/hc/en-us) tools. Annotated SNPs in the mouse (or human) *dbsnp* (ftp.ncbi.nlm.nih.gov/snp/) and sanger mouse genomes project (https://www.sanger.ac.uk/data/mouse-genomes-project/), were filtered from variant calls prior to further analysis. The computational pipeline for picard and GATK, and code for processing variant tables and plotting is available at https://github.com/lukedow/iBE.git.

Immunohistochemistry and immunofluorescence

Tissue was fixed, processed, and imaged as previously described [54]. IDEXX RADIL performed H&E on paraffin embedded sections. For immunofluorescence (IF), primary antibodies used were: rabbit anti-Cas9 (CST, #19526), mouse anti-p53 (CST, #2524), mouse anti-Glutamine synthetase (GS; BD Transduction Labs #610517), mouse anti-β-catenin (CST, #2698), rabbit anti-Cytokeratin-19 (CK19, Abcam, #ab133496), and rabbit anti- alpha Smooth muscle actin (aSMA, Abcam, #ab5694), rabbit anti-RFP (Rockland, AB_2209751), chicken anti-GFP (Abcam, #ab13970), rabbit anti-P-AKT (CST, #4060). Secondary antibodies used were donkey anti-rabbit 594 (1:500, Invitrogen, #A21207) and donkey anti-mouse 647 (Invitrogen, #A31571). All IF sections were counterstained with DAPI.

Hydrodynamic teil vein injections

1ug SB13 transposase, 5ug SB-*Myc*, and gRNA (20ug plasmid gRNA or 2nmol Synthego synthetic standard chemically modified or 2nmol Synthego synthetic heavily modified gRNA[58]) in 2mL saline was delivered by lateral teil vein injection over 5–7s in 8–12 week old mice. Tumors were harvested after palpation and at a humane endpoint.

Pancreas electroporation

Surgery to perform *in vivo* electroporation is previously described [59, 60]. In brief, the surgical site is scrubbed with a povidone-iodine scrub (e.g., Betadine®, Nolvasan®), and the site is then rinsed with 70% alcohol. Under isofluorane (2–3%) anesthetization, a

small laparotomy is performed and the pancreas is luxated with a blunt forceps. 5ug SB13 transposase, 25ug SB-*Kras*^{G12D}, and gRNA (20ug gRNA plasmid or 2nmol Synthego synthetic, heavily modified gRNA[58]) in 30uL total volume (saline used to normalize) were delivered by injection into the pancreas. Solution is injected using a 27.5 gauge needle and tweezer electrodes are tightly placed around the injection bubble. Two pulses of electrical current using an *in vivo* electroporator (NEPAGENE NEPA21 Type II *in vitro* and *in vivo* electroporator) are applied. After electroporation, the peritoneum cavity is rinsed with 0.5ml of pre-warmed saline. Subsequently the peritoneum and muscles are sutured with absorbable sutures and the skin is closed with skin staples. The mice are kept at 37C until they are awake and post-surgery pain management is done with injections of buprenorphine for the three following days (twice daily). Surgery and electroporation were performed on 8–12 week old mice. Tumors were harvested after palpation and at a humane endpoint.

Statistical Analysis

All statistical tests used are indicated in the corresponding figure legends. In general, to compare two conditions, a standard two-tailed unpaired *t* test was used, assuming variance between samples. In most cases, analyses were performed with one-way or two-way ANOVA, with Tukey's correction for multiple comparisons. Unless otherwise stated, each replicate represents an independent mouse/organoid lines or tumors from $n \geq 3$ mice. Experimenters were not blinded to conditions. All statistics are reported in Supplementary Table 5.

Extended Data

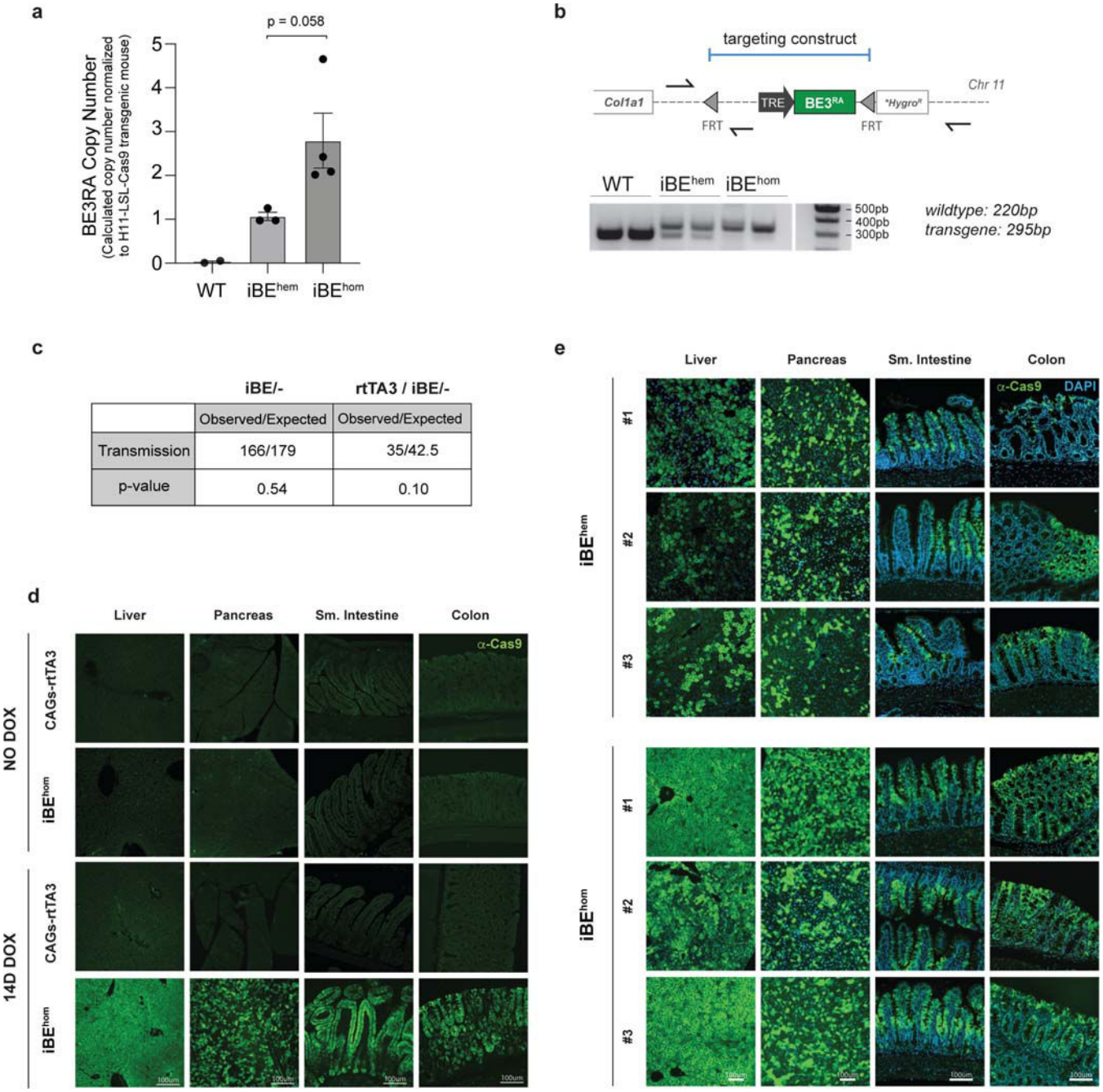

Extended Figure 1: Regulatable BE expression *in vivo*

a. Calculated BE3RA transgene copy number in iBE^{hem} and iBE^{hom} using a Taqman quantiative PCR assay with genomic DNA from H11-LSL-Cas9 mice as a reference. Data are presented as mean values ± s.e.m. (*p<0.05, Student's t-test). **b.** Schematic representation of the targeted RMCE site downstream of the Col1a1 locus. Primers flanking the knock-in cassette and a single primer within the targeted transgene can identify wildtype, hemizygous and homozygous animals, as shown in the example genotyping agarose gel

c. Mendelian transmission of Col1a1-targeted iBE knock-in (with and without R26-CAGs-rtTA3 allele) and associated p-value (chi-square test) relative to expected Mendelian inheritance. **d.** Immunofluorescent detection of Cas9 protein in rtTA3 only and iBE^{hom} mice maintained on normal chow (No dox) or doxycycline chow for 14 days (14D dox). (n=3 mice per genotype and condition). **e.** Immunofluorescent detection of Cas9 protein in iBE^{hem} (top) or iBE^{hom} (bottom) mice maintained on dox chow for 7 days across four tissues. (n=3 mice per genotype and condition).

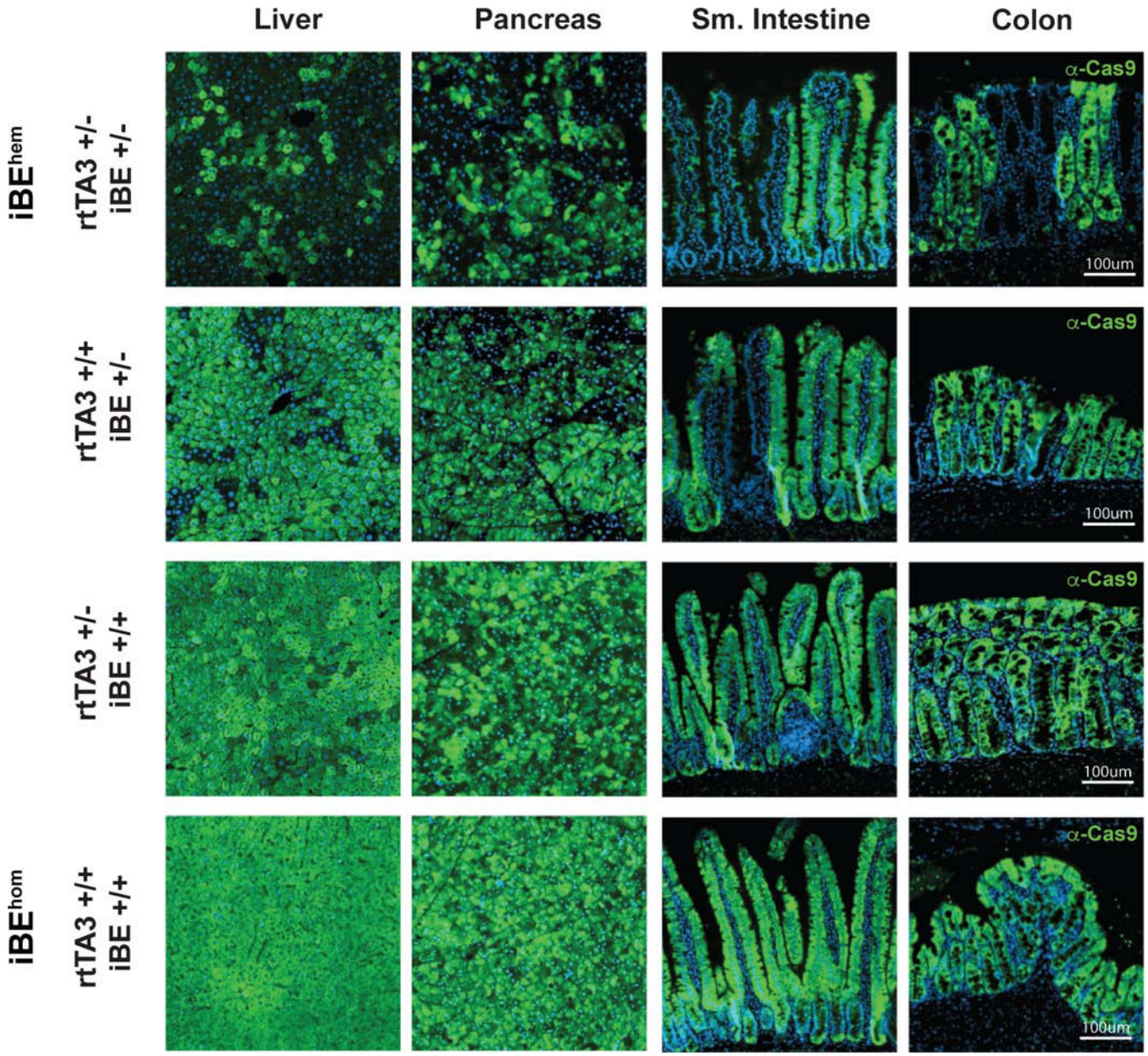

Extended Figure 2: Expression of BE3RA across different tissues in mice carrying one or two copy of each allele.

Immunofluorescent detection of Cas9 protein in rtTA3$^{+/-}$ iBE$^{+/-}$ (iBE^{hem}), rtTA3$^{+/+}$ iBE$^{+/-}$, rtTA3$^{+/-}$ iBE$^{+/+}$ and rtTA3$^{+/+}$iBE$^{+/+}$ (iBE^{hom}) mice maintained on dox chow for 14 days.

Cas9 protein(green), DAPI staining for nuclei (blue) across four tissues analyzed. (n=3 mice per genotype and condition).

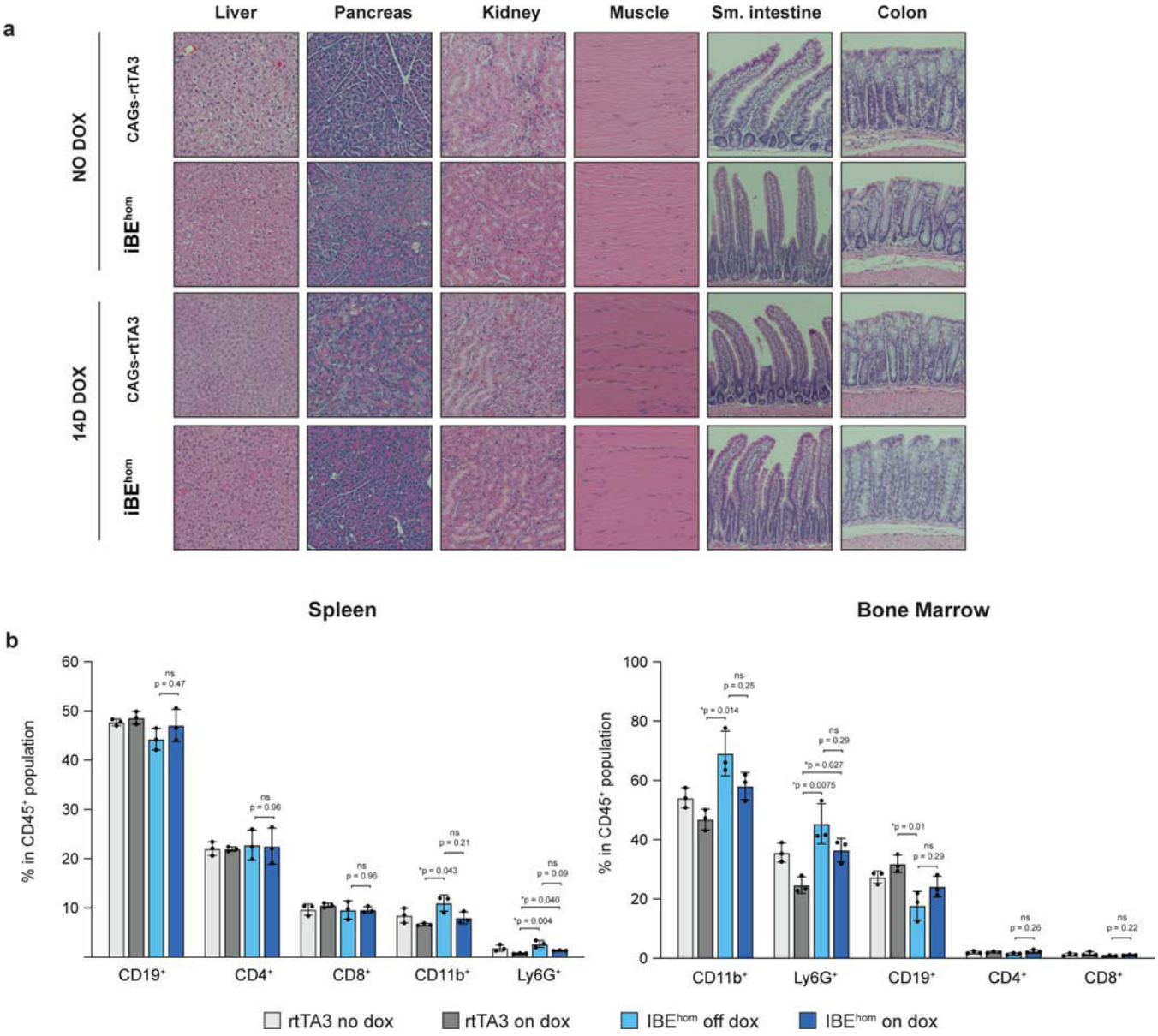

Extended Figure 3: Dox treatment does not induce abnormalities in iBE^{hom} mice.

a. Hematoxylin and Eosin (H&E) staining in rtTA3$^{+/-}$iBE$^{-/-}$ and rtTA3$^{+/+}$iBE$^{+/+}$ (iBE^{hom}) on normal chow or doxycycline chow for 14 days. (n=3 mice). **b.** Flow cytometry analysis of spleen and bone marrow cell suspensions of rtTA3$^{+/-}$iBE$^{-/-}$ and rtTA3$^{+/+}$iBE$^{+/+}$ (iBE^{hom}) on normal chow or maintained on doxycycline chow for 14 days (n=3 mice). Data are presented as mean values ± s.d (*p<0.05, Student's t-test).

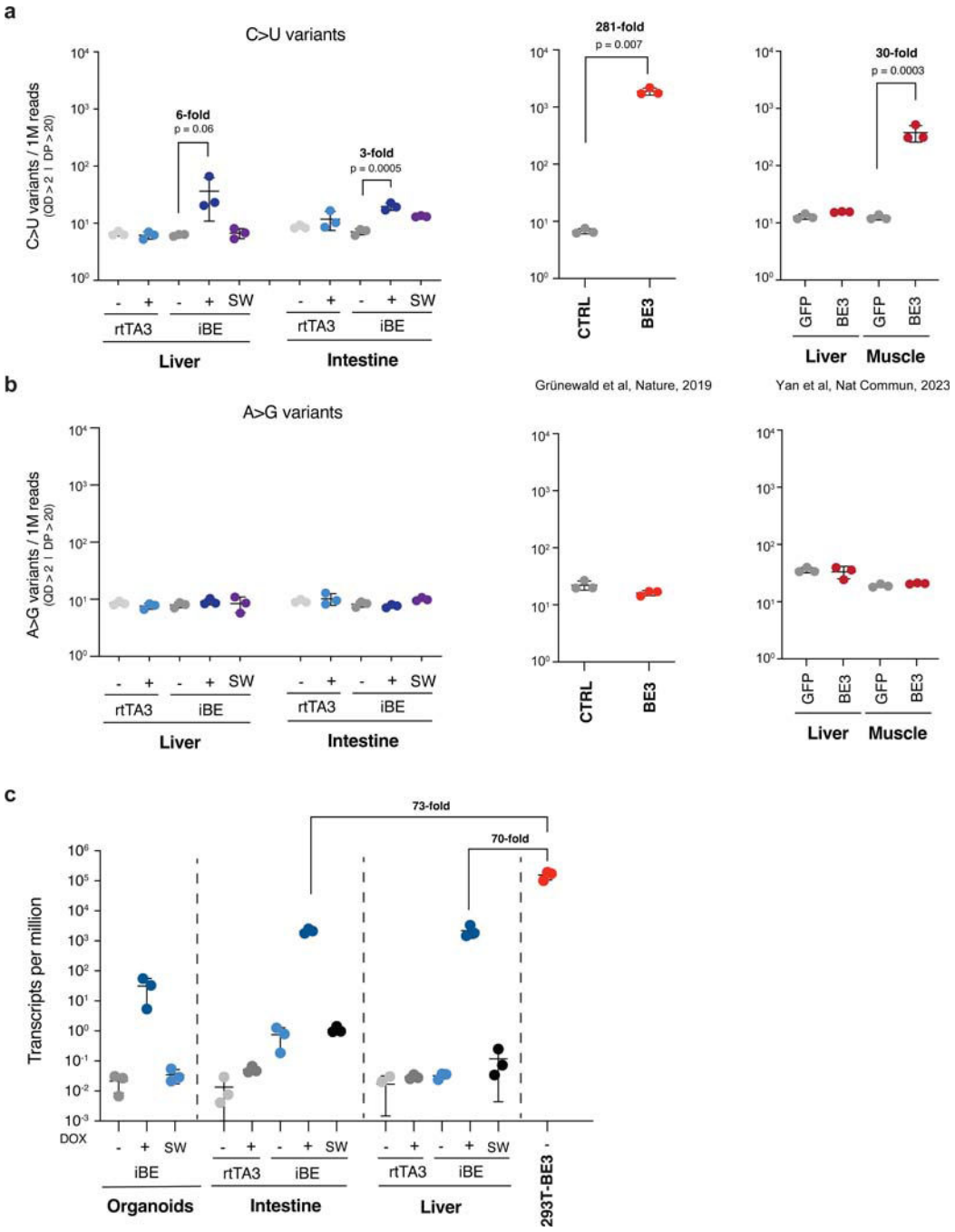

Extended Figure 4: iBE induces low off target RNA editing that is reversed by withdrawal of transgene expression.

a. C to U editing in RNA transcripts detected from RNA sequencing data from intestine and liver from rtTA^{hem} and iBE^{hom} on normal chow (−), dox chow (+) for 14 days, or switched from dox chow for 14 days to normal chow for 6 days (SW). Data in the middle and right panels was derived from re-analysis of published datasets, as indicated under each plot. For experiments with multiple comparisons, p-values were calculated by one-way ANOVA, n=3 mice/condition. For individual pairwise comparisons, Student's t-test was used. **b.** A to G

editing in RNA transcripts detected from RNA sequencing data from intestine and liver from rtTAhem and iBEhom on normal chow (−), dox chow (+) for 14 days, or switched from dox chow for 14 days to normal chow for 6 days (SW). (n=3 mice). **c.** Transcript abundance (transcripts per million; TPM) in pancreatic organoids, intestine, and liver from $rtTA^{hem}$ and iBE^{hom} on normal chow (−), dox chow (+) for 14 days, or switched from dox chow for 14 days to normal chow for 6 days (SW). All data shown are presented as mean values +/− s.d., n=3 mice/condition.

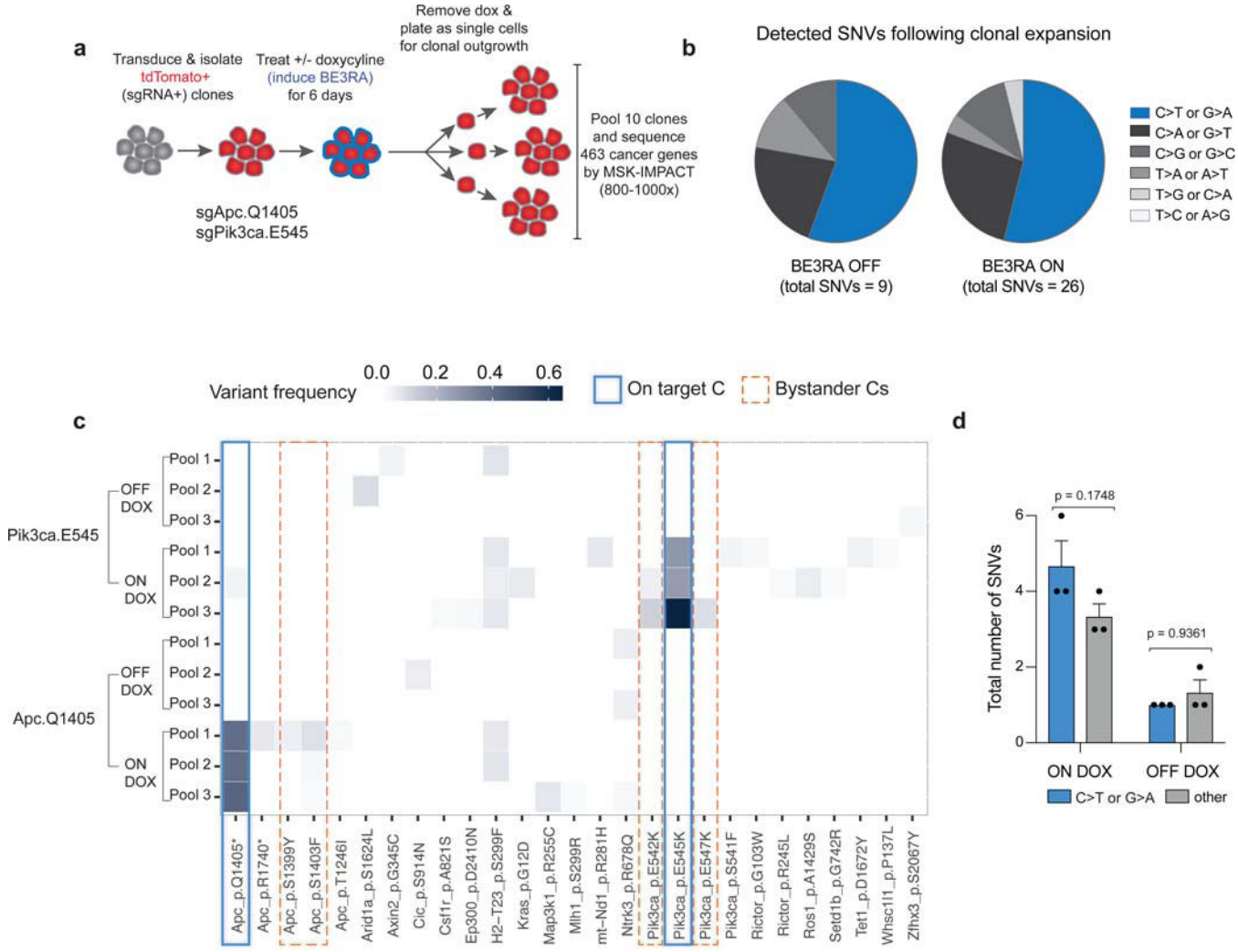

Extended Figure 5. iBE has low DNA off target activity.

a. Schematic of experimental set up in mouse embryonic stem cells (ESCs). mESCs containing iBE knock in were transduced with LRT2B-gRNA vector and selected for gRNA expression. sgRNA+ cells were plated with and without dox for 6 days after which cells were plated at low density for clonal outgrowth without dox. 3 pools of 10 clones were picked for each dox conditions across to gRNA targeted cell lines (sgRNAs = Apc.Q1405X and Pik3ca.E545K). In total, 12 pools of 10 clones were sequenced at 800–1000-fold coverage across the MSK-IMPACT cancer gene set. **b.** Pie chart display of frequency of C>T or C>other SNVs found in pooled clones for each condition (on and off dox) for both

sgRNAs. **c.** Sequencing analysis at cancer gene sites in cell conditions (right) described in a. Solid blue boxes represent on-target activity of the sgRNA, dotted orange boxes signify on-target 'bystander' editing within the gRNA window. **d.** Quantification of C>T and C>other SNVs found across both targets. 2-way ANOVA test for multiple comparisons was used to evaluate statistical significance across conditions. Data are presented as mean values ± s.e.m. p-values are displayed.

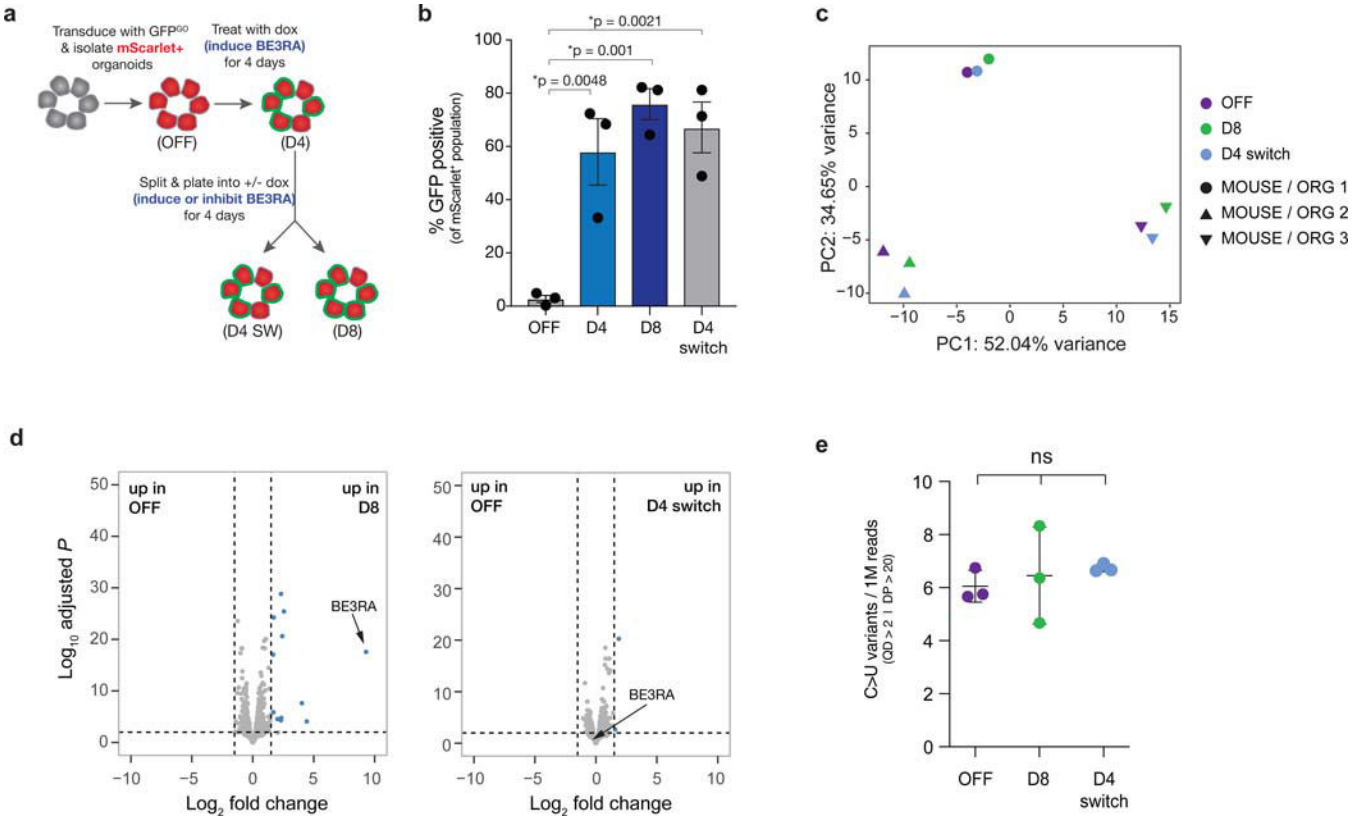

Extended Figure 6: iBE does not induce off target RNA editing in organoids.

a. Schematic of experimental set up in iBE derived pancreatic organoids. Organoids were transduced and selected with GFP^{GO} reporter ($mScarlet^{+}$). Organoids maintained off dox were then split into dox conditions to induce BE expression for 4 days and then split again into + and – dox conditions for an additional day. **b.** Editing of organoids in each condition (OFF, D4, D8, and D4 sw) was quantified by flow cytometry, calculating the percentage of GFP^{+} cells within the $mScarlet^{+}$ population. Data are presented as mean values ± s.e.m. One-way ANOVA with Tukey's correction **c.** PCA analysis of RNA sequencing data from OFF, D8, and D4 SW organoids. Colors correspond to dox condition and shape delineates organoid replicate/mouse origin (n=3). **d.** Volcano plots from RNA-seq data comparing iBE pancreatic organoids culture on dox-containing media vs regular media. **e**. Off-target RNA editing analysis, processed as described for Supplementary Figure 4. No significant differences in RNA variants were observed, n=3, one-way ANOVA with Tukey's correction. Data are presented as mean values ± s.e.m. For all data shown, n=3 independent organoid lines/condition.

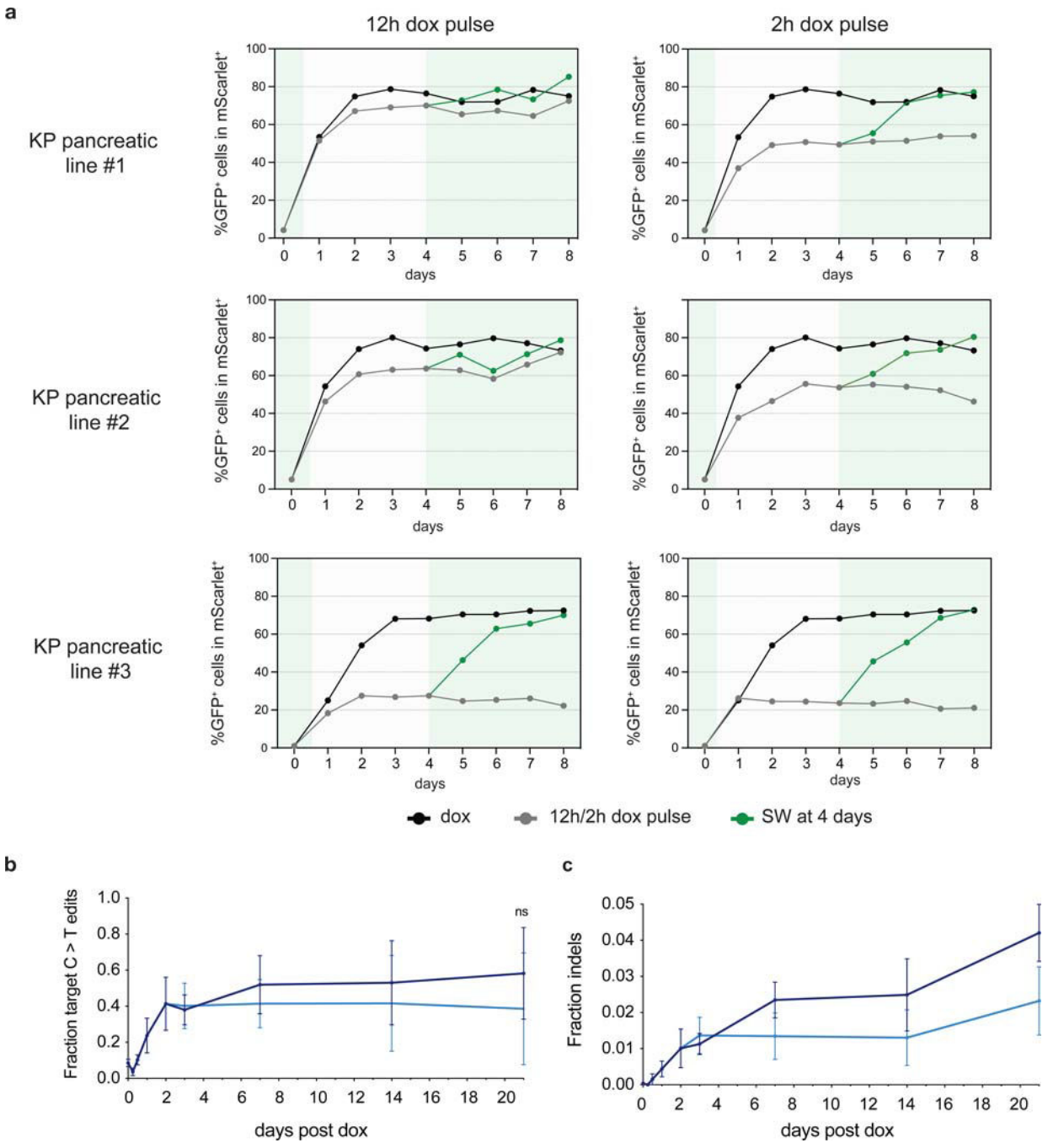

Extended Figure 7: Editing dynamics of iBE organoids.

a. Flow cytometry analysis of three independent pancreatic KP mutant organoid lines integrated with GFP^{GO} reporter following dox treatment for 0–8 days (black), transient exposure for 2h or 12h (grey), or transient exposure then re-treatment at 4 days (green). **b.** Targeted deep sequencing quantification of target C:G to T:A conversion at the ApcQ1405X locus in 2D small intestinal derived iBE cell line following dox addition for 21 days (dark blue), or transient dox treatment for 3 days and withdrawn for 18 days (light blue). **c.**

Targeted deep sequencing quantification of indel conversion of b. Data are presented as mean values ± s.e.m. (*p<0.05, Student's t-test) (n=3 independently derived line).

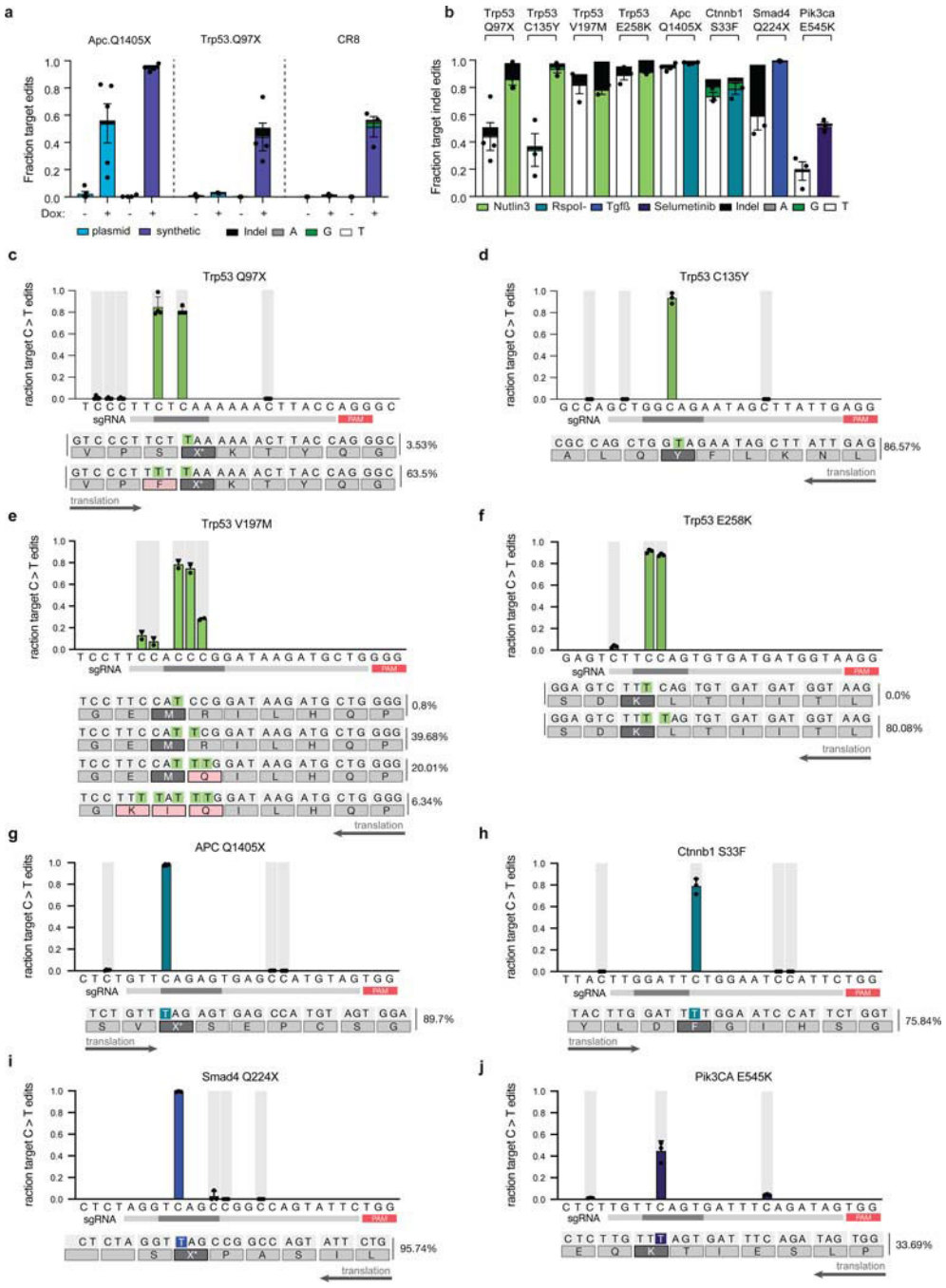

Extended Figure 8: Efficient BE in iBE organoids with low collateral editing.

a. Targeted deep sequencing quantification of corresponding target C>T/A/G and indel conversion in small intestinal iBE organoids nucleofected with plasmid (light blue) or synthetic (indigo) gRNAs (ApcQ1405, Trp53Q97, CR8.OS2) as indicated, with and without dox treatment. **b.** Targeted deep sequencing quantification of target C>T/A/G and indel

conversion in small intestinal iBE organoids nucleofected with synthetic gRNAs targeting cancer associated SNVs from Figure 2f. **c-j.** Quantification of collateral editing of adjacent cytosines for samples shown in Figure 2f. Predicted translation of each quantified read is shown below with targeted amino acid substitution (dark grey) and additional amino acid substitution (pink). All data are presented as mean values ± s.e.m.

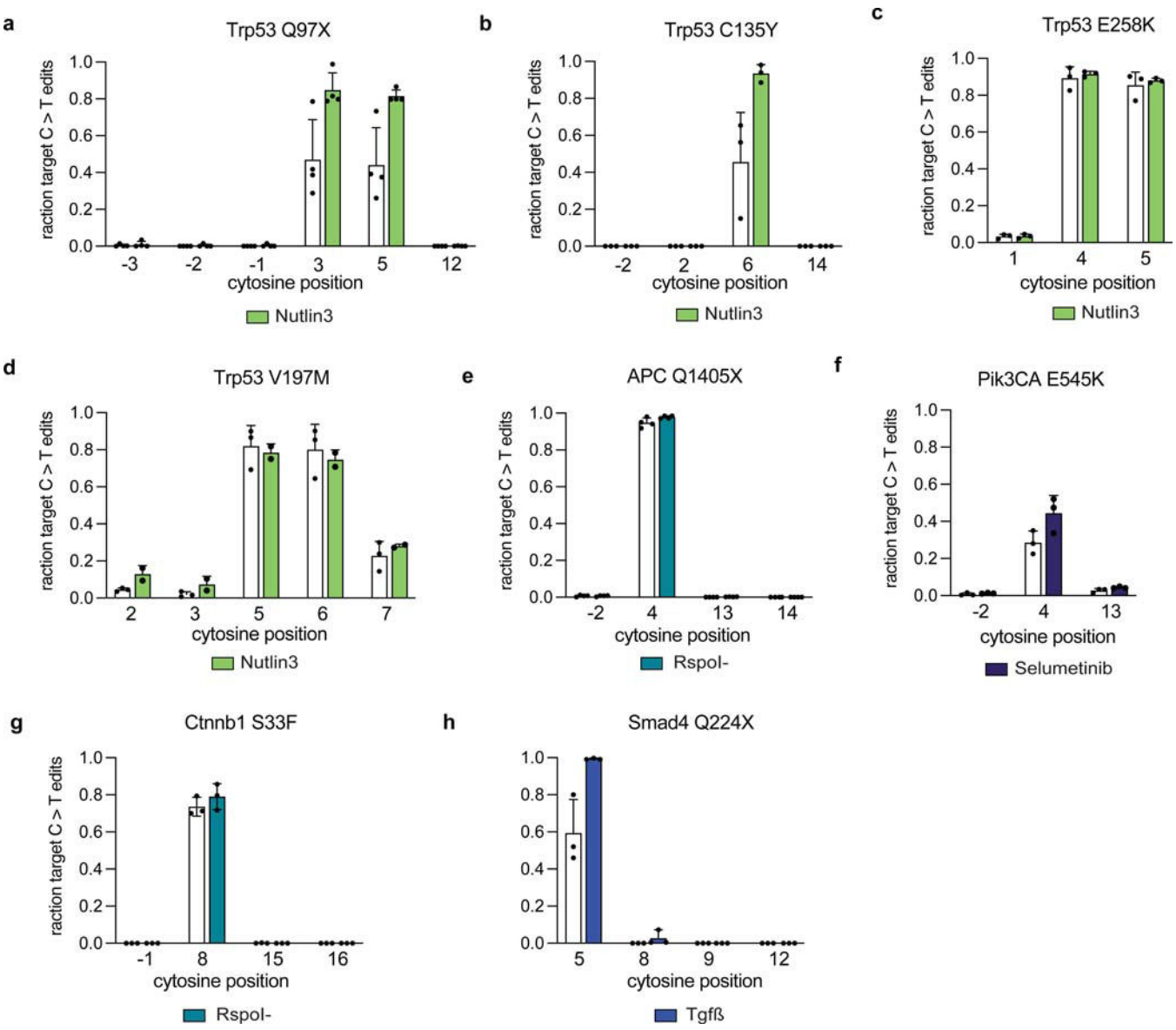

Extended Figure 9: Analysis of collateral editing before and after functional selection.

a-h. Quantification of collateral editing of adjacent cytosines for data shown in Figure 2f, unselected (white) and selected (color) in small intestinal iBE organoids nucleofected with various synthetic gRNAs targeting cancer associated SNVs.

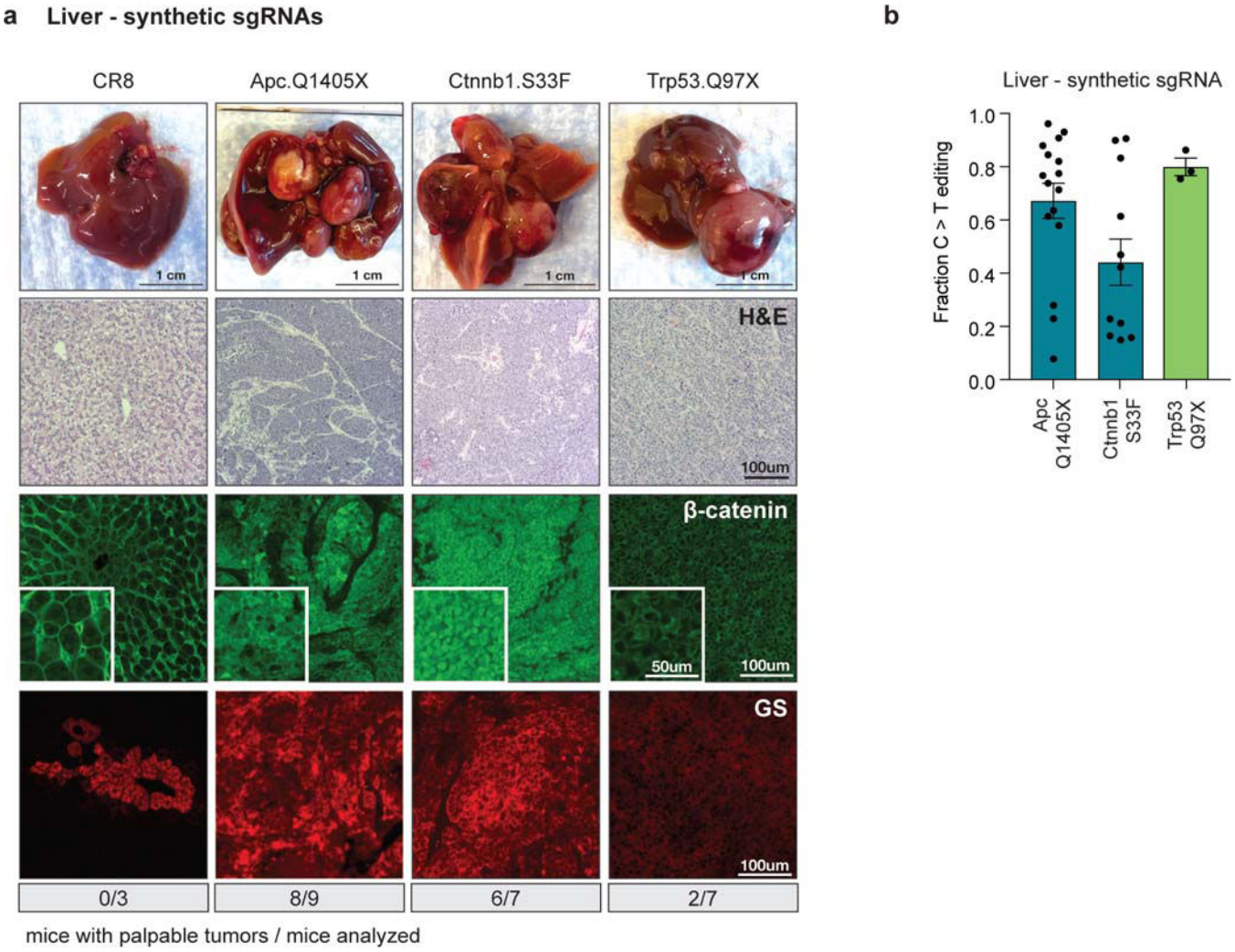

Extended Figure 10. In situ base editing with iBE by synthetic gRNA delivery drives liver tumors.

a. HTVI delivery of synthetic gRNAs with *SB-Myc* as in Figure 4. BF, H&E images, and IF staining for ß-catenin (green) and glutamine synthetase (GS, red) in livers with tumors. Number of transfected mice with palpable tumors is shown below each column.

b. Quantification of target C:G to T:A conversion from tumors described in a). Each point corresponds to an isolated bulk tumor. (n=2–7 mice for a given gRNA target). Individual editing data color-coded by animal in Supplementary Figure 3. All data are presented as mean values ± s.e.m.

Supplementary Material

Refer to Web version on PubMed Central for supplementary material.

Acknowledgements

We thank members of the Dow lab for advice and comments on preparation of the manuscript. We would like to acknowledge Kaloyan Tsanov and Josef Leibold for assistance and advice in setting up the pancreas EPO protocol.

The content is solely the responsibility of the authors and does not necessarily represent the official views of the NIH.

Funding

This work was supported by a project grant from the National Institutes of Health (NIH/NCI; R01CA229773), P01 CA087497 (SWL), a MSKCC Functional Genomics Initiative (FGI) grant (SWL), and an Agilent Technologies Thought Leader Award (SWL), and support from Synthego Inc. under a Synthego Innovator Award (LED). A.K. was supported by an F31 Ruth L. Kirschstein Predoctoral Individual National Research Service Award (F31–CA247351–02). A.V was supported by a Human Frontier Scientific Program (HFSP) Postdoctoral Fellowship. B.J.D. was supported by an F31 Ruth L. Kirschstein Predoctoral Individual National Research Service Award (F31–CA261061–01). E.E.G. is the Kenneth G. and Elaine A. Langone Fellow of the Damon Runyon Cancer Research Foundation (DRG–2343–18). FJSR was supported by the MSKCC TROT program (5T32CA160001), a GMTEC Postdoctoral Researcher Innovation Grant, and is an HHMI Hanna Gray Fellow. SWL is an HHMI investigator.

Conflicts of interest

L.E.D. is a scientific advisor and holds equity in Mirimus Inc. L.E.D. has received consulting fees and/or honoraria from Volastra Therapeutics, Revolution Medicines, Repare Therapeutics, Fog Pharma, and Frazier Healthcare Partners. S.W.L is an advisor for and has equity in the following biotechnology companies: ORIC Pharmaceuticals, Faeth Therapeutics, Blueprint Medicines, Geras Bio, Mirimus Inc., PMV Pharmaceuticals, and Constellation Pharmaceuticals. SWL acknowledges receiving funding and research support from Agilent Technologies for the purposes of massively parallel oligo synthesis. K.H., A.P.K, and J.A.W are employees and shareholders of Synthego Corporation.

Data availability

All source data (including P values) are available in Supplementary Table 5. Raw fastq files have been deposited in the sequence read archive (SRA) under accession PRJNA859154. Processed RNAseq data (TPM values and differentially expressed genes) is available in Supplementary Table 2.

Code availability

Code for analysis and data visualization is available at: https://github.com/lukedow/iBE.git.

References

1. Goodwin S, McPherson JD & McCombie WR. Coming of age: ten years of next-generation sequencing technologies. Nat Rev Genet 17, 333–351 (2016). [PubMed: 27184599]
2. Landrum MJ et al. ClinVar: public archive of interpretations of clinically relevant variants. Nucleic Acids Res 44, D862–868 (2016). [PubMed: 26582918]
3. Vogelstein B et al. Cancer genome landscapes. Science 339, 1546–1558 (2013). [PubMed: 23539594]
4. Vivanco I et al. Differential sensitivity of glioma- versus lung cancer-specific EGFR mutations to EGFR kinase inhibitors. Cancer Discov 2, 458–471 (2012). [PubMed: 22588883]
5. Hyman DM et al. AKT Inhibition in Solid Tumors With AKT1 Mutations. J Clin Oncol 35, 2251–2259 (2017). [PubMed: 28489509]
6. Vasan N et al. Double PIK3CA mutations in cis increase oncogenicity and sensitivity to PI3Kalpha inhibitors. Science 366, 714–723 (2019). [PubMed: 31699932]
7. Findlay GM et al. Accurate classification of BRCA1 variants with saturation genome editing. Nature 562, 217–222 (2018). [PubMed: 30209399]
8. Zafra MP et al. Optimized base editors enable efficient editing in cells, organoids and mice. Nat Biotechnol 36, 888–893 (2018). [PubMed: 29969439]
9. Komor AC, Kim YB, Packer MS, Zuris JA & Liu DR. Programmable editing of a target base in genomic DNA without double-stranded DNA cleavage. Nature 533, 420–424 (2016). [PubMed: 27096365]

10. Gaudelli NM et al. Programmable base editing of A*T to G*C in genomic DNA without DNA cleavage. Nature 551, 464–471 (2017). [PubMed: 29160308]
11. Gaudelli NM et al. Directed evolution of adenine base editors with increased activity and therapeutic application. Nat Biotechnol 38, 892–900 (2020). [PubMed: 32284586]
12. Komor AC et al. Improved base excision repair inhibition and bacteriophage Mu Gam protein yields C:G-to-T:A base editors with higher efficiency and product purity. Sci Adv 3, eaao4774 (2017).
13. Rothgangl T et al. In vivo adenine base editing of PCSK9 in macaques reduces LDL cholesterol levels. Nat Biotechnol 39, 949–957 (2021). [PubMed: 34012094]
14. Villiger L et al. In vivo cytidine base editing of hepatocytes without detectable off-target mutations in RNA and DNA. Nat Biomed Eng 5, 179–189 (2021). [PubMed: 33495639]
15. Villiger L et al. Treatment of a metabolic liver disease by in vivo genome base editing in adult mice. Nat Med 24, 1519–1525 (2018). [PubMed: 30297904]
16. Song C-Q et al. Adenine base editing in an adult mouse model of tyrosinaemia. Nature Biomedical Engineering (2019).
17. Yeh WH, Chiang H, Rees HA, Edge ASB & Liu DR. In vivo base editing of post-mitotic sensory cells. Nat Commun 9, 2184 (2018). [PubMed: 29872041]
18. Banskota S et al. Engineered virus-like particles for efficient in vivo delivery of therapeutic proteins. Cell 185, 250–265 e216 (2022). [PubMed: 35021064]
19. Ryu SM et al. Adenine base editing in mouse embryos and an adult mouse model of Duchenne muscular dystrophy. Nat Biotechnol 36, 536–539 (2018). [PubMed: 29702637]
20. Yang L et al. Amelioration of an Inherited Metabolic Liver Disease through Creation of a De Novo Start Codon by Cytidine Base Editing. Mol Ther 28, 1673–1683 (2020). [PubMed: 32413280]
21. Dow LE et al. Conditional reverse tet-transactivator mouse strains for the efficient induction of TRE-regulated transgenes in mice. PLoS One 9, e95236 (2014).
22. Premsrirut PK et al. A rapid and scalable system for studying gene function in mice using conditional RNA interference. Cell 145, 145–158 (2011). [PubMed: 21458673]
23. Grunewald J et al. CRISPR DNA base editors with reduced RNA off-target and self-editing activities. Nat Biotechnol 37, 1041–1048 (2019). [PubMed: 31477922]
24. Yan N et al. Cytosine base editors induce off-target mutations and adverse phenotypic effects in transgenic mice. Nat Commun 14, 1784 (2023). [PubMed: 36997536]
25. Zehir A et al. Mutational landscape of metastatic cancer revealed from prospective clinical sequencing of 10,000 patients. Nat Med 23, 703–713 (2017). [PubMed: 28481359]
26. Zafra MP et al. An In Vivo Kras Allelic Series Reveals Distinct Phenotypes of Common Oncogenic Variants. Cancer Discov 10, 1654–1671 (2020). [PubMed: 32792368]
27. Schatoff EM et al. Distinct CRC-associated APC mutations dictate response to Tankyrase inhibition. Cancer Discov (2019).
28. Katti A et al. GO: a functional reporter system to identify and enrich base editing activity. Nucleic Acids Res 48, 2841–2852 (2020). [PubMed: 32112097]
29. Sanchez-Rivera FJ et al. Base editing sensor libraries for high-throughput engineering and functional analysis of cancer-associated single nucleotide variants. Nat Biotechnol 40, 862–873 (2022). [PubMed: 35165384]
30. Mehta A & Merkel OM. Immunogenicity of Cas9 Protein. J Pharm Sci 109, 62–67 (2020). [PubMed: 31589876]
31. Chew WL et al. A multifunctional AAV-CRISPR-Cas9 and its host response. Nat Methods 13, 868–874 (2016). [PubMed: 27595405]
32. Wang D et al. Adenovirus-Mediated Somatic Genome Editing of Pten by CRISPR/Cas9 in Mouse Liver in Spite of Cas9-Specific Immune Responses. Human gene therapy 26, 432–442 (2015). [PubMed: 26086867]
33. Ruiz de Galarreta M et al. beta-catenin activation promotes immune escape and resistance to anti-PD-1 therapy in hepatocellular carcinoma. Cancer Discov (2019).

34. Calvisi DF et al. Activation of the canonical Wnt/beta-catenin pathway confers growth advantages in c-Myc/E2F1 transgenic mouse model of liver cancer. J Hepatol 42, 842–849 (2005). [PubMed: 15885355]
35. Hingorani SR et al. Trp53R172H and KrasG12D cooperate to promote chromosomal instability and widely metastatic pancreatic ductal adenocarcinoma in mice. Cancer Cell 7, 469–483 (2005). [PubMed: 15894267]
36. Alsner J et al. A comparison between p53 accumulation determined by immunohistochemistry and TP53 mutations as prognostic variables in tumours from breast cancer patients. Acta Oncol 47, 600–607 (2008). [PubMed: 18465328]
37. Freed-Pastor WA & Prives C. Mutant p53: one name, many proteins. Genes Dev 26, 1268–1286 (2012). [PubMed: 22713868]
38. Bartek J, Iggo R, Gannon J & Lane DP. Genetic and immunochemical analysis of mutant p53 in human breast cancer cell lines. Oncogene 5, 893–899 (1990). [PubMed: 1694291]
39. Maresch R et al. Multiplexed pancreatic genome engineering and cancer induction by transfection-based CRISPR/Cas9 delivery in mice. Nature Communications 7, 10770 (2016).
40. Park JS et al. Pancreatic cancer induced by in vivo electroporation-enhanced sleeping beauty transposon gene delivery system in mouse. Pancreas 43, 614–618 (2014). [PubMed: 24713671]
41. Annunziato S et al. In situ CRISPR-Cas9 base editing for the development of genetically engineered mouse models of breast cancer. EMBO J, e102169 (2020).
42. Zhou C et al. Off-target RNA mutation induced by DNA base editing and its elimination by mutagenesis. Nature 571, 275–278 (2019). [PubMed: 31181567]
43. Arbab M et al. Determinants of Base Editing Outcomes from Target Library Analysis and Machine Learning. Cell 182, 463–480 e430 (2020). [PubMed: 32533916]
44. Marquart KF et al. Predicting base editing outcomes with an attention-based deep learning algorithm trained on high-throughput target library screens. Nat Commun 12, 5114 (2021). [PubMed: 34433819]
45. Pallaseni A et al. Predicting base editing outcomes using position-specific sequence determinants. Nucleic Acids Res 50, 3551–3564 (2022). [PubMed: 35286377]
46. Park J & Kim HK. Prediction of Base Editing Efficiencies and Outcomes Using DeepABE and DeepCBE. Methods Mol Biol 2606, 23–32 (2023). [PubMed: 36592305]
47. Kim Y et al. High-throughput functional evaluation of human cancer-associated mutations using base editors. Nat Biotechnol 40, 874–884 (2022). [PubMed: 35411116]
48. Winters IP et al. Multiplexed in vivo homology-directed repair and tumor barcoding enables parallel quantification of Kras variant oncogenicity. Nat Commun 8, 2053 (2017). [PubMed: 29233960]
49. Bock D et al. In vivo prime editing of a metabolic liver disease in mice. Sci Transl Med 14, eabl9238 (2022).
50. Davis JR et al. Efficient prime editing in mouse brain, liver and heart with dual AAVs. Nat Biotechnol (2023).
51. Dow LE et al. A pipeline for the generation of shRNA transgenic mice. Nat Protoc 7, 374–393 (2012). [PubMed: 22301776]
52. O'Rourke KP, Ackerman S, Dow LE & Lowe SW. Isolation, Culture, and Maintenance of Mouse Intestinal Stem Cells. Bio Protoc 6 (2016).
53. Huch M et al. Unlimited in vitro expansion of adult bi-potent pancreas progenitors through the Lgr5/R-spondin axis. Embo j 32, 2708–2721 (2013). [PubMed: 24045232]
54. Zafra MP et al. An in vivo KRAS allelic series reveals distinct phenotypes of common ocogenic variants. Cancer Discovery In Press (2020).
55. Amen AM et al. Endogenous spacing enables co-processing of microRNAs and efficient combinatorial RNAi. Cell Reports Methods.
56. Dobin A et al. STAR: ultrafast universal RNA-seq aligner. Bioinformatics 29, 15–21 (2013). [PubMed: 23104886]
57. Love MI, Huber W & Anders S. Moderated estimation of fold change and dispersion for RNA-seq data with DESeq2. Genome Biol 15, 550 (2014). [PubMed: 25516281]

58. Finn JD et al. A Single Administration of CRISPR/Cas9 Lipid Nanoparticles Achieves Robust and Persistent In Vivo Genome Editing. Cell Reports 22, 2227–2235 (2018). [PubMed: 29490262]

59. Paffenholz Stella V et al. Senescence induction dictates response to chemo- and immunotherapy in preclinical models of ovarian cancer. Proceedings of the National Academy of Sciences 119, e2117754119 (2022).

60. Leibold J et al. Somatic Tissue Engineering in Mouse Models Reveals an Actionable Role for WNT Pathway Alterations in Prostate Cancer Metastasis. Cancer Discov 10, 1038–1057 (2020). [PubMed: 32376773]

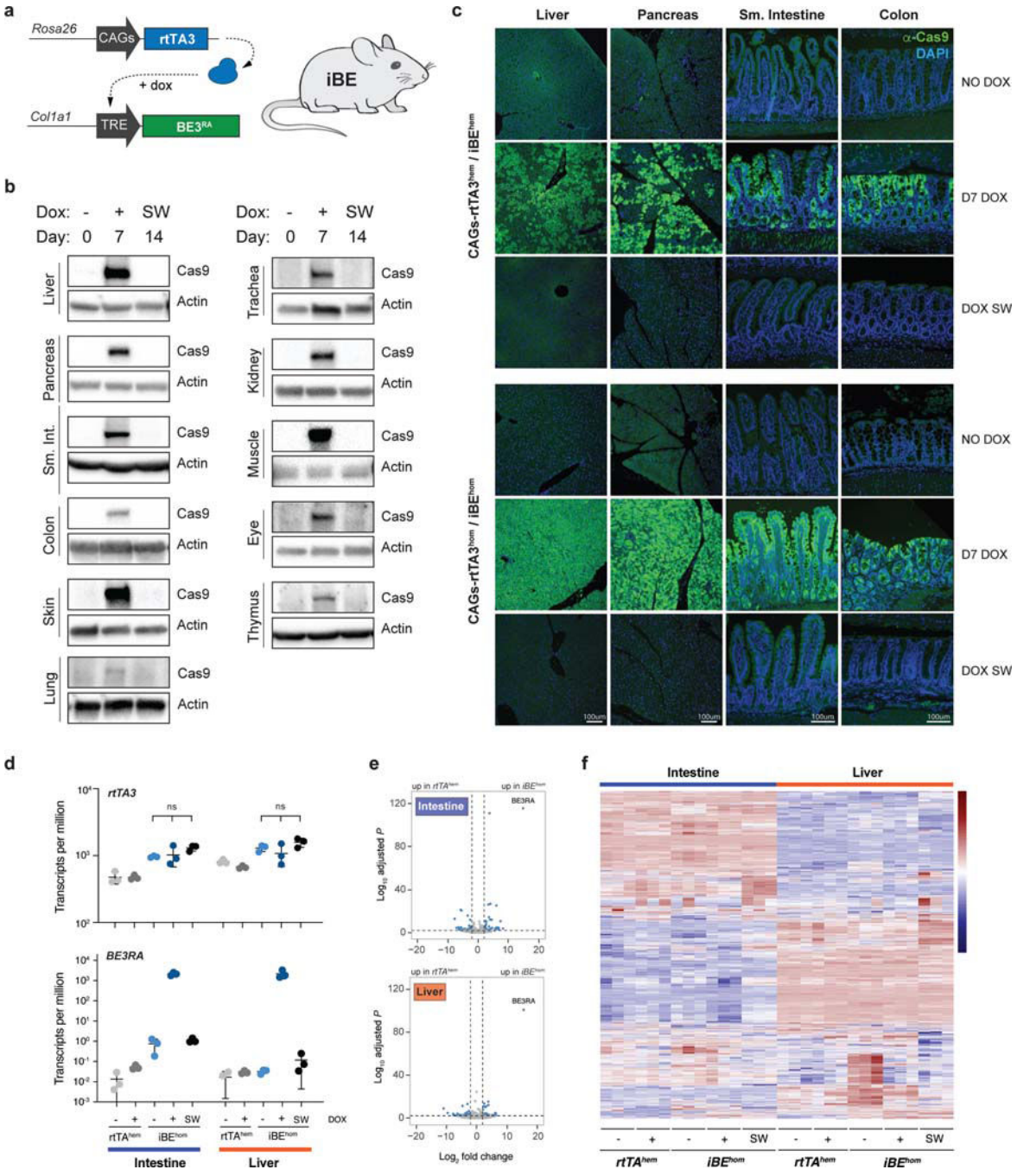

Figure 1. Regulatable BE expression across murine tissues

a. Schematic representation of iBE mice containing *R26-CAGs-rtTA3* allele and *TRE-BE3RA* allele. **b.** Cas9 immunoblot on bulk tissue, as indicated, from iBE^{hem} mice maintained on normal chow (Day 0, - dox), doxycycline chow for 7 days (Day7, + dox), or dox switched from doxycycline chow for 7 days to normal chow for 7 days (D14, -dox) across tissues bulk harvested for protein. ß-actin, loading control. Molecular weight: β-actin (42kDa), BE3RA (160kDa). Blots are representative of 2 independent experiments for each condition. **c.** Immunofluorescent detection of Cas9 protein in iBE^{hem} (top) or

iBE^{hom} (bottom) mice maintained on normal chow (No dox) or doxycycline chow for 7 days (Day 7 Dox) or dox switched from dox chow for 7 days to normal chow for 7 days (Dox SW). Cas9 protein (green), DAPI staining for nuclei (blue) across four tissues analyzed. Data is representative of 3 independent mice for each condition – see Extended Data Fig. 1e for individual replicates. **d.** Transcript abundance (transcripts per million, TPM) in intestine and liver from rtTA^{hem} and iBE^{hom} on normal chow (−), dox chow (+) for 14 days, or switched from dox chow for 14 days to normal chow for 6 days (SW). Data are presented as mean values ± s.d., n=3 mice per genotype/condition. **e.** Volcano plots from RNA-seq data comparing rtTA^{hem} vs iBE^{hom} maintained on dox chow for 14 day (n=3 mice). **f.** Heat map of differentially expressed (DE) genes from intestine and liver from rtTA^{hem} and iBE^{hom} on normal chow (−), dox chow (+) for 14 days, or switched from dox chow for 14 days to normal chow for 6 days (SW). Includes DE gene between all conditions within the intestine and liver groups; does not include differentially expressed genes between different tissues (n=3 mice per genotype/condition).

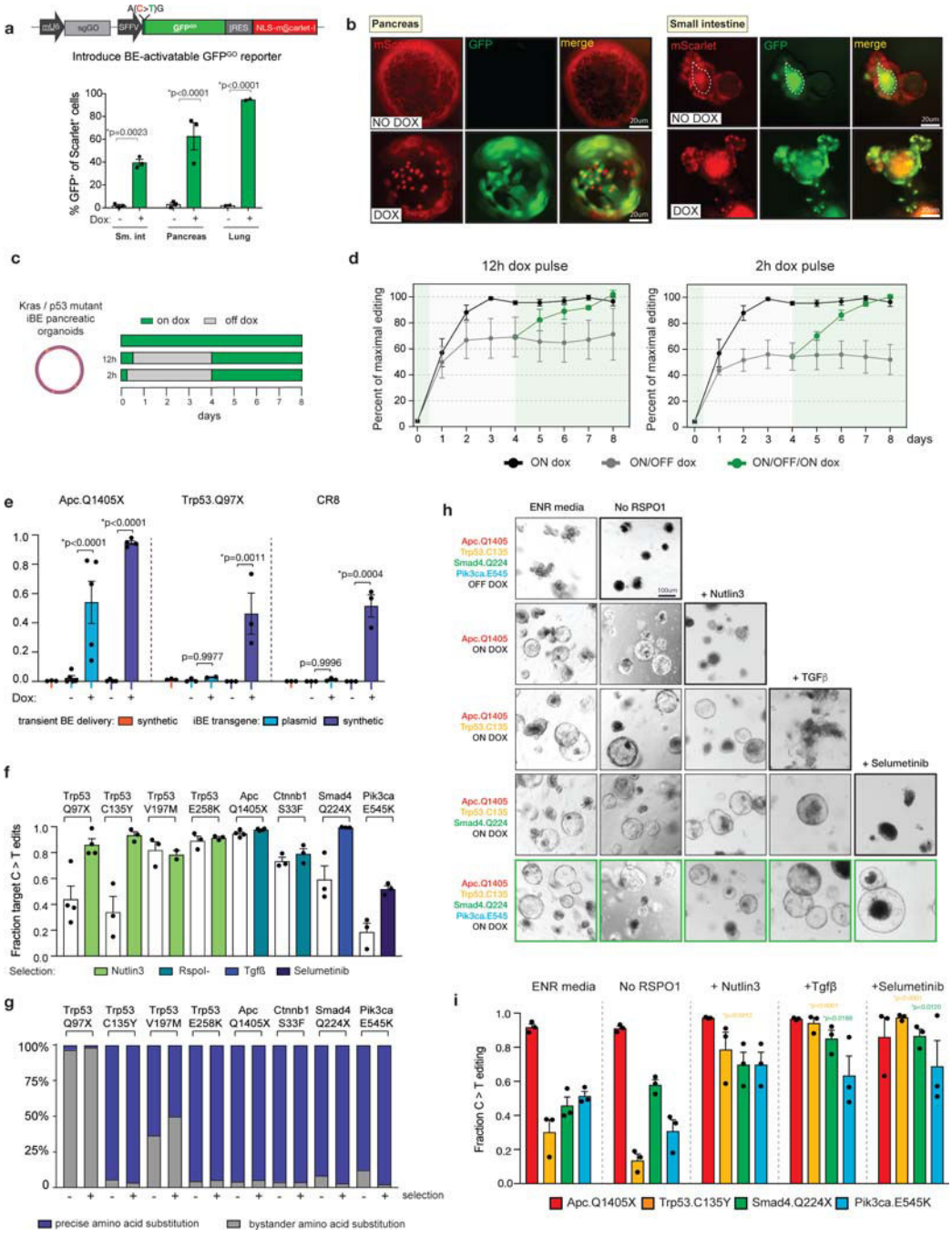

Figure 2. Efficient base editing in ex vivo derived iBE organoids

a. Schematic of GFP^{GO} reporter and quantitation of BE-mediated GFP activation in mScarlet^{+} organoids with and without dox by flow cytometry. **b.** Live fluorescence imaging of small intestinal and pancreatic organoids containing stable integration of GFP^{GO} lentiviral construct cultured without (no dox) or with dox. Dotted white line indicates central lumen of small intestinal organoids that produce bright autofluorescent signal. **c.** Schematic for dox treatment of KP pancreatic organoids to assess editing dynamics. **d.** Flow cytometry analysis of pancreatic KP mutant organoids integrated with GFP^{GO} reporter following:

continual dox treatment (0–8 days) (black), transient exposure to dox for 12h/2h (grey), or transient treatment and then re-exposure to dox in the same cells (green) (n=3 independently derived organoid cultures) **e.** Targeted deep sequencing quantification of target C:G to T:A conversion in small intestinal iBE organoids nucleofected with plasmid (light blue) or synthetic (indigo) gRNAs (ApcQ1405, Trp53Q97, CR8.OS2) as indicated, and WT organoids nucleofected with synthetic sgRNAs and an optimized BE (FNLS) cDNA plasmid (orange). **f.** Targeted deep sequencing quantification of target C:G to T:A conversion in dox-treated small intestinal iBE organoids nucleofected with various synthetic gRNAs as indicated, and either unselected (−) or selected with corresponding functional selective media condition. **g.** Frequency of precise amino acid substitution in small intestinal iBE organoids nucleofected with synthetic gRNAs in f. **h.** Brightfield images of small intestinal iBE organoids targeted with various gRNA combinations and dox conditions (left) taken through sequential selection of RspoI withdrawal, Nutlin3; Tgfß, and Selumetinib. Bolded black boxes are conditions failing to survive selection. Bolded green boxes indicate quadruple targeted organoids (with dox) surviving all four selection conditions. Images representative of 3 independently derived intestinal organoid cultures. **i.** Targeted deep sequencing quantification of target C:G to T:A conversion (and C> other or indels) in small intestinal iBE organoids nucleofected with 4 synthetic gRNAs in e (green boxes) at each gRNA target loci (ApcQ1405, Trp53C135, Smad4Q224, Pik3caE545. Media conditions and corresponding organoid genotype and sequencing information is grouped and listed above (n=3, p-values derived from one-way ANOVA with Tukey’s correction for multiple testing). All data are presented as mean values ± s.e.m. All experiments describing iBE organoids include three independently derived organoid cultures.

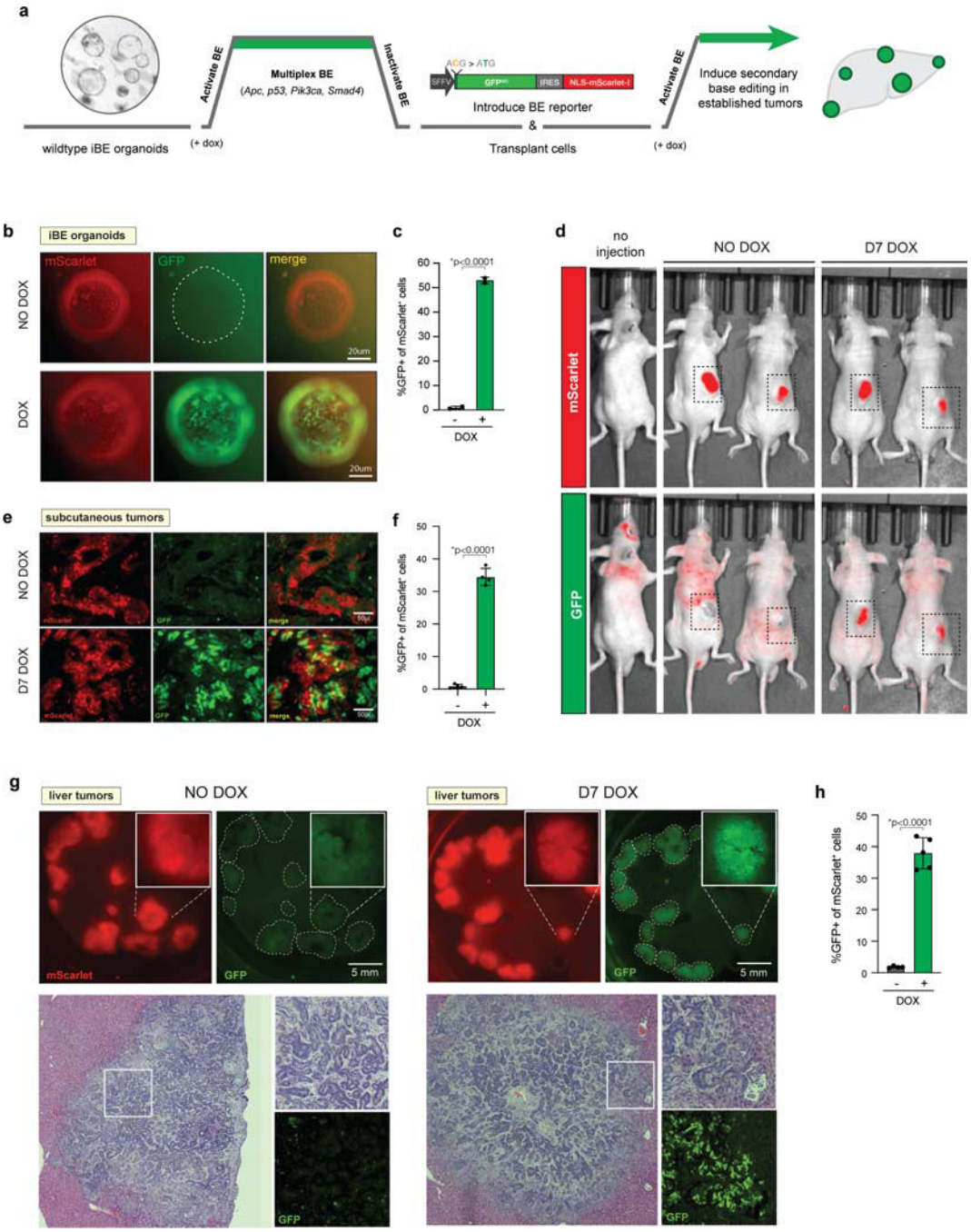

Figure 3: iBE enables sequential base editing *in vitro* and *in vivo*.

a. Schematic representation of the experimental workflow for sequential base editing in vivo. Wildtype small intestinal organoids were isolated from iBE^{hom} mice and treated with dox to induce the BE alongside with synthetic sgRNA to engineer 4 oncogenic single nucleotide variants (as shown in Figure 2h). Dox was withdrawn to silence BE expression and a 5th sgRNA was introduced in a lentiviral vector carrying the GFP^{GO} fluorescent BE reporter. Organoids were engrafted into the flanks or livers of recipient mice and tumors were allowed to form 10 days for sub-cutaneous injection or 8 weeks for liver engraftment.

Mice were treated with systemic dox (in the chow) for 1 week to induce BE expression. **b.** Fluorescence imaging of quadruple mutant small intestine organoids containing stable integration of GFP^{GO} reporter cultured without (no dox) or with dox. **c.** Quantification by flow cytometry of GFPGO activation in mScarlet+ organoids with and without dox from b. Data are presented as mean values ± s.e.m. (n=5 mice per condition) (*p<0.05, Student's t-test, unpaired, two-sided). d. *In vivo* fluorescence imaging of mice containing subcutaneous tumors maintained on normal chow (No dox) or doxycycline chow for 7 days (D7 Dox). **e.** Immunohistochemical detection of GFP and mScarlet in subcutaneous tumors harvested from mice maintained on normal chow (No dox) or doxycycline chow for 7 days (D7 Dox). **f.** Quantification by flow cytometry of GFP^{GO} activation in enzymatically digested subcutaneous tumors with and without dox. Data are presented as mean values ± s.e.m. (n=5 mice per condition) (*p<0.05, Student's t-test, unpaired, two-sided). **g.** Wholemount fluorescence, H&E and immunohistochemical detection of GFP and mScarlet in liver tumors harvested from mice maintained on normal chow (No dox) or doxycycline chow for 7 days (D7 Dox). **h.** Quantification by flow cytometry of GFP^{GO} activation in dissected and enzymatically digested liver tumors from g. Data are presented as mean values ± s.e.m. (n=5 mice per condition) (*p<0.05, Student's t-test, unpaired, two-sided).

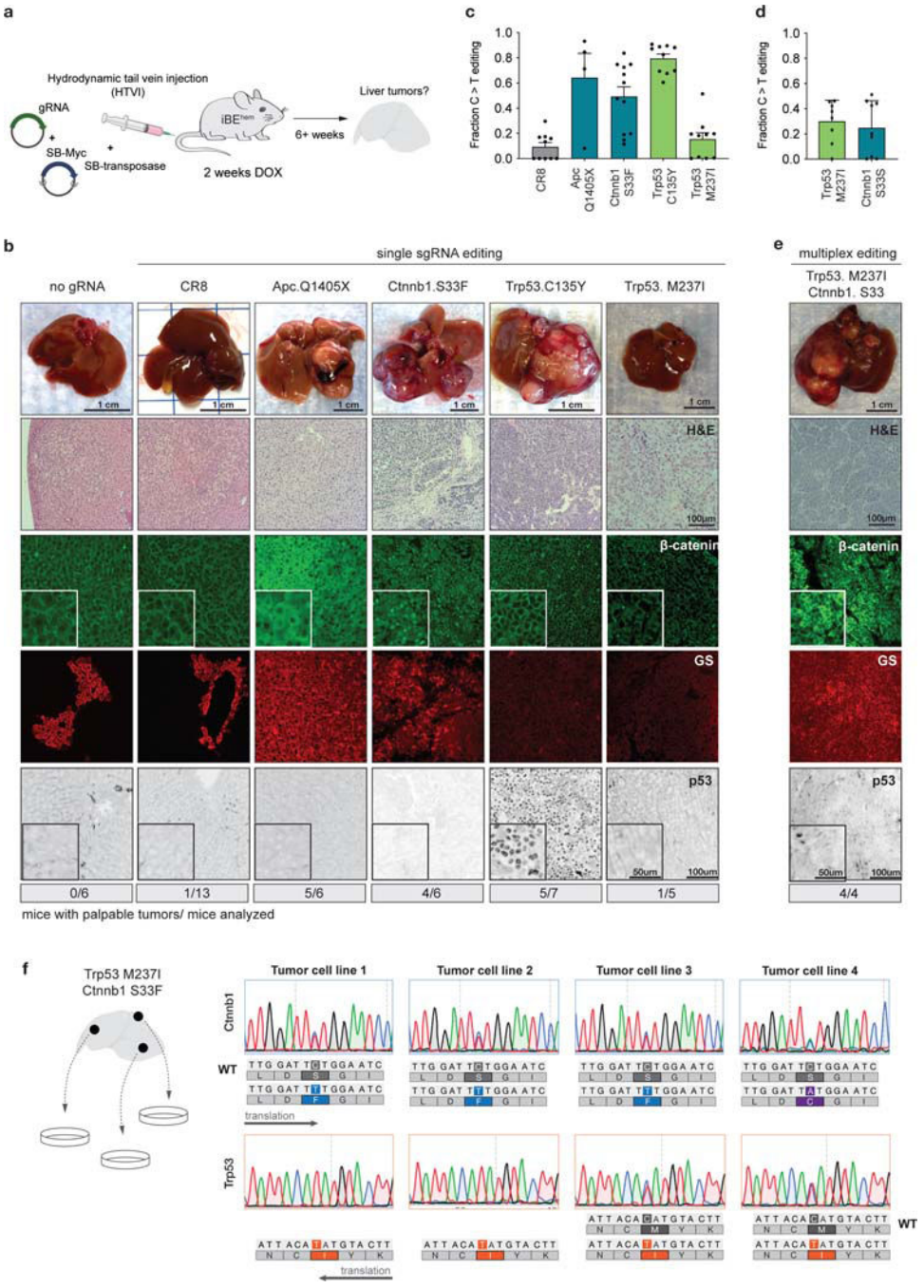

Figure 4: In situ base editing with iBE drives liver tumors.

a. Schematic for experimental setup of hydrodynamic teil vein (HTVI) injection mediated delivery of plasmid gRNA and sleeping beauty transposon mediated integration of cMyc cDNA (SB-Myc) in the liver of iBE mice maintained on dox for 1 week surrounding injection. Post injection, mice are monitored for tumor development and palpable tumors are harvested for tumor histological and sequencing analysis. **b.** Brightfield images of liver after harvest targeted according to the experimental pipeline in a) and with the corresponding gRNA listed (top). Hematoxylin and eosin (H&E) staining (2nd row) of corresponding

liver lesions. Immunohistochemical staining of total ß catenin (green, 3rd row), glutamine synthetase (GS, red, 4th row) and p53 (black, 5th row). Fraction of number of mice with palpable tumors over number of mice injected is below each column. **c-d.** Targeted deep sequencing analysis of target C:G to T:A conversion in individual dissected tumors collected in 'b' delineated by sgRNA/target site for individual (**c**) or multiplexed (**d**) experiments. Each point corresponds to a physically isolated individual bulk tumor; n=3 mice minimum for a given sgRNA target. Individual editing data color-coded by animal is shown in Supplementary Figure 3. Data are presented as mean values ± s.e.m. **e.** Brightfield images of liver after multiplexed delivery of SB-Myc and both $Trp53^{M237I}$ and $Ctnnb1^{S33F}$ sgRNAs. **f.** Sequencing of target sites of cell lines derived from individual liver tumor isolated from mice targeted with both $Ctnnb1^{S33F}$ and $Trp53^{M237I}$. Predicted translation of sequenced regions is shown below with WT amino acid (grey) and targeted amino acid substitution for Ctnnb1 (blue) and Trp53 (orange).

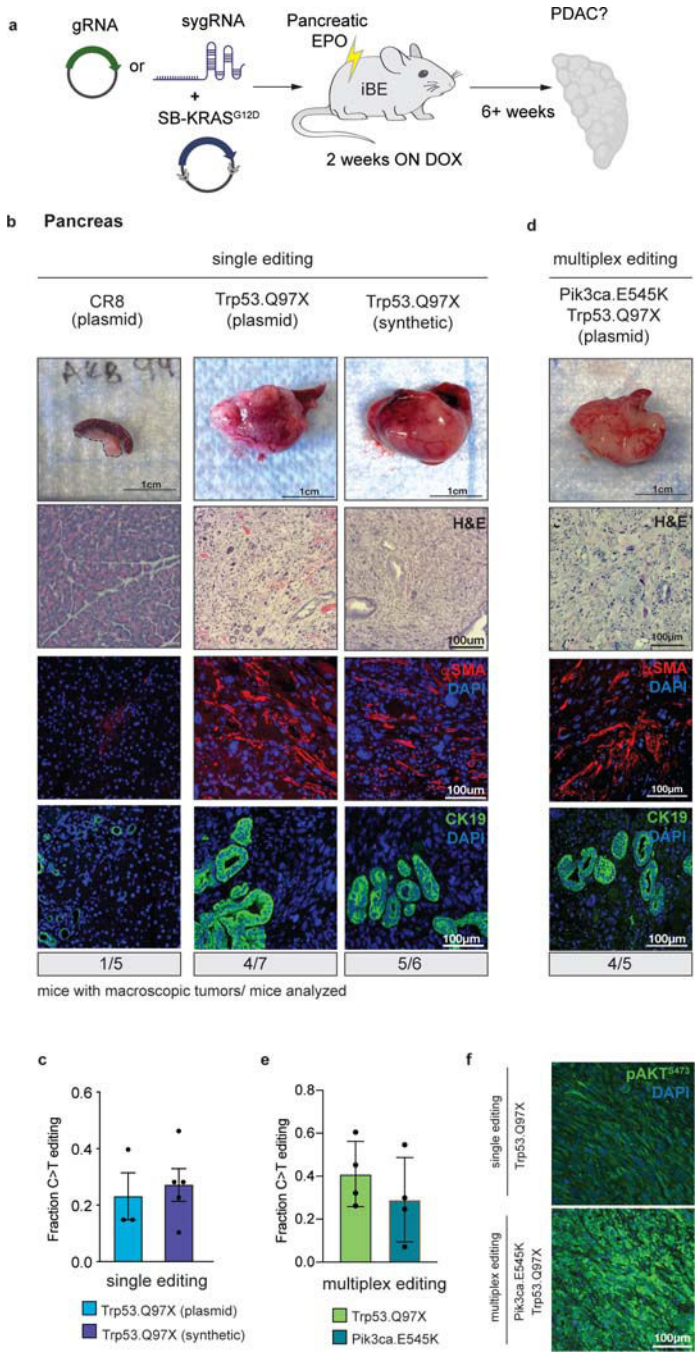

Figure 5. Efficient engineering of missense mutations in pancreatic tumor models.

a. Schematic for experimental setup of pancreatic electroporation mediated delivery of gRNA and sleeping beauty transposon mediated integration of KrasG12D cDNA (SB-Kras) in the pancreas of iBE^{hom} mice maintained on dox for 2 weeks surrounding electroporation. Post electroporation, mice are monitored for tumor development and palpable tumors are harvested for tumor histological and sequencing analysis. **b.** Brightfield images of pancreas tumor with spleen attached (top row) using plasmid or synthetic gRNA. Hematoxylin and eosin (H&E) staining (2nd row) of pancreatic tumors electroporated as in panel (a) for

gRNAs listed. Immunohistochemical staining of alpha smooth muscle actin (aSMA, red, 3rd row) and cytokeratin-19 (CK19, green, 4th row) counterstained with DAPI (blue). Number of mice with palpable tumors over number of mice injected is below each column. **c.** Targeted deep sequencing analysis of target C:G to T:A conversion in tumors collected in b) for plasmid gRNA (left) and synthetic gRNA (right). Each point corresponds to one mouse analyzed. (n=3 mice minimum for a given gRNA target). Data are presented as mean values ± s.e.m. **d.** Brightfield images of pancreas tumor with spleen attached (top row) using plasmid gRNA targeting both Trp53Q97X and Pik3caE545. **e.** Targeted deep sequencing analysis of target C:G to T:A conversion in pancreatic tumors collected using plasmid gRNA targeting both Trp53Q97X and Pik3caE545. Each point corresponds to one mouse analyzed. (n=4). Data are presented as mean values ± s.e.m. **f.** Immunohistochemical staining of $pAKT^{S473}$ in pancreatic tumors using gRNA targeting Trp53Q97X alone or both Trp53Q97X and Pik3caE545. Image shown is representative of n=4 independent tumors analyzed.